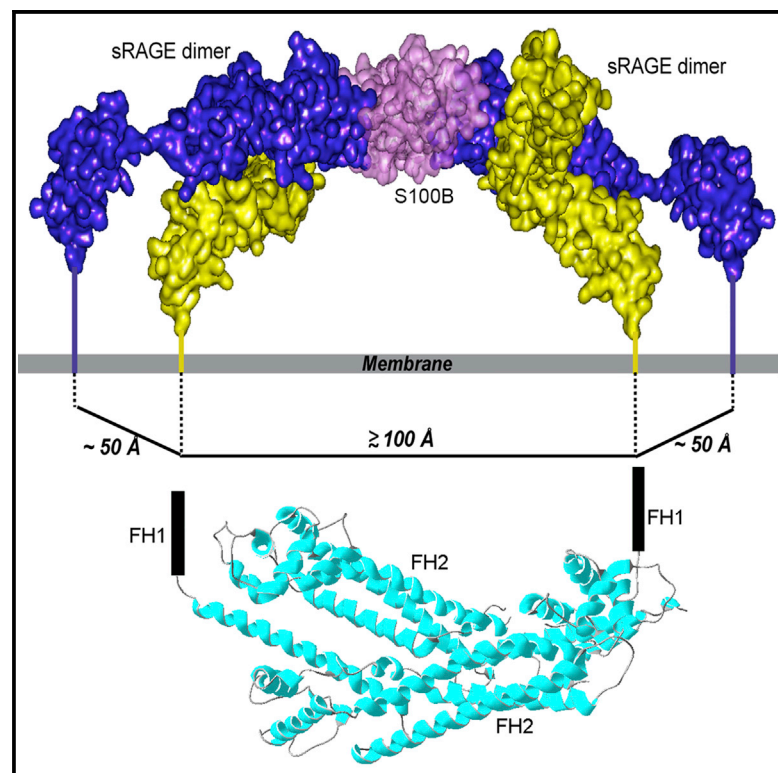


Structure

Change in the Molecular Dimension of a RAGE-Ligand Complex Triggers RAGE Signaling

Graphical Abstract



Authors

Jing Xue, Michael Manigrasso, Matteo Scalabrin, ..., Daniele Fabris, Ann Marie Schmidt, Alexander Shekhtman

Correspondence

ashekhtman@albany.edu

In Brief

RAGE is a signaling molecule central to the induction and perpetuation of inflammatory responses. The dimerization interaction surfaces on RAGE are identified. Structural modeling suggests that ligand-induced association of dimers on the cell surface increases the molecular dimension of the receptor to recruit Diaphanous 1 and activate signaling pathways.

Highlights

- NMR spectroscopy, cross-linking, and MS were used to construct a model of RAGE dimers
- Dimers and larger oligomers can form by utilizing the same interacting surfaces
- Oligomerization and ligand binding increase the molecular dimension of RAGE
- The increase in molecular dimension promotes signal transduction

Change in the Molecular Dimension of a RAGE-Ligand Complex Triggers RAGE Signaling

Jing Xue,¹ Michaele Manigrasso,² Matteo Scalabrin,¹ Vivek Rai,³ Sergey Reverdatto,¹ David S. Burz,¹ Daniele Fabris,¹ Ann Marie Schmidt,² and Alexander Shekhtman^{1,*}

¹Department of Chemistry, State University of New York at Albany, Albany, NY 12222, USA

²New York University, Langone Medical Center, New York, NY 10016, USA

³Institute of Life Sciences, Bhubaneswar, Odisha 751023, India

*Correspondence: ashekhtman@albany.edu

<http://dx.doi.org/10.1016/j.str.2016.06.021>

SUMMARY

The weak oligomerization exhibited by many transmembrane receptors has a profound effect on signal transduction. The phenomenon is difficult to characterize structurally due to the large sizes of and transient interactions between monomers. The receptor for advanced glycation end products (RAGE), a signaling molecule central to the induction and perpetuation of inflammatory responses, is a weak constitutive oligomer. The RAGE domain interaction surfaces that mediate homo-dimerization were identified by combining segmental isotopic labeling of extracellular soluble RAGE (sRAGE) and nuclear magnetic resonance spectroscopy with chemical cross-linking and mass spectrometry. Molecular modeling suggests that two sRAGE monomers orient head to head forming an asymmetric dimer with the C termini directed toward the cell membrane. Ligand-induced association of RAGE homo-dimers on the cell surface increases the molecular dimension of the receptor, recruiting Diaphanous 1 (DIAPH1) and activating signaling pathways.

INTRODUCTION

Oligomerization is common among cell-surface receptors in resting as well as signal transduction active states and appears to be critical for receptor function (Metzger, 1992). Oligomerization is observed in such diverse families of receptors as immunoreceptors (Ramsland et al., 2011), T cell receptors (Berry et al., 2011; Choudhuri et al., 2005), B cell receptors (Schamel and Reth, 2000), growth factors (DiGabriele et al., 1998), and hormone receptors (Angers et al., 2002). Oligomerization is triggered by the inter-molecular engagement of extracellular and/or intracellular domains. Expressed separately, extracellular domains are usually only weakly oligomeric and thus present a difficult target to characterize structurally.

A constitutive oligomer, the receptor for advanced glycation end products (RAGE), is a member of the immunoglobulin (Ig) superfamily of cell-surface receptors (Neeper et al., 1992; Schmidt et al., 1992; Xie et al., 2007). RAGE consists of three extracellular

Ig domains, a V-type Ig domain (residues 23–119) and two C-type Ig domains (C1 and C2) (residues 120–233 and residues 234–325, respectively), a transmembrane helix, and a short cytoplasmic tail. RAGE signaling plays a central role in the inflammatory response, mediating aspects of immunity, acute and chronic inflammatory disorders, complications of diabetes, and certain cancers (Hofmann et al., 1999; Liliensiek et al., 2004; Medapati et al., 2015; Schmidt et al., 2001; Taguchi et al., 2000; van Zoelen et al., 2009). As a pattern recognition receptor (Xie et al., 2008), RAGE binds diverse families of ligands, including advanced glycation end products (Kislinger et al., 1999; Neeper et al., 1992; Xie et al., 2008; Xue et al., 2011), S100/calgranulins (Hofmann et al., 1999; Koch et al., 2010), High Mobility Group Box-1 (HMGB1) (Taguchi et al., 2000) proteins, amyloid- β peptides (A β), β -sheet fibrils (Yan et al., 1996), lysophosphatidic acid (Rai et al., 2012b), and phosphatidylserine (He et al., 2011). Ligand binding to extracellular RAGE domains is tightly coupled to the recruitment of Diaphanous 1 (DIAPH1) to the cytoplasmic domain and the generation of reactive oxygen species (Bianchi et al., 2011; Hudson et al., 2008; Toure et al., 2012), which contribute to RAGE-dependent pathological processes, such as growth, migration, and secretion of inflammatory cytokines.

Structural studies of extracellular soluble RAGE (sRAGE), which consists of the V, C1, and C2 domains, revealed that the C-terminal C2 domain is structurally independent of the slightly bent, elongated structure of the joined V and C1 domains, which together form an integrated structural unit, the VC1 domain (Dattilo et al., 2007; Koch et al., 2010; Park et al., 2010; Yatime and Andersen, 2013). The oligomeric states of sRAGE, inferred from the crystal structures of isolated VC1 (Koch et al., 2010) (Xu et al., 2013) and VC1C2 domains (Yatime and Andersen, 2013), are inconsistent with solution studies of sRAGE oligomers (Sarkany et al., 2011; Sitkiewicz et al., 2013). Studying the isolated domains can misrepresent sRAGE oligomerization because electrostatic forces between neutral sRAGE monomers ($pI = 7.8$) are vastly different from those between isolated positively charged VC1 domains ($pI = 9.9$) and negatively charged C2 domains ($pI = 4.2$).

We combined solution nuclear magnetic resonance (NMR) spectroscopy of segmentally labeled sRAGE (Camarero et al., 2002; Dawson et al., 1994; Xue et al., 2012) with chemical cross-linking analyzed by mass spectrometry as a means to overcome the shortcomings of studying weakly associating oligomers. By incorporating limited experimental measurements, a reliable structural model was computed, and a mechanism for

signal transduction was proposed and examined by cellular activity studies of fluorescently labeled RAGE and its intracellular effector DIAPH1.

RESULTS

Segmentally Labeled, Chemically Ligated CL-sRAGE Is Functional

Segmentally labeling large multidomain proteins simplifies NMR spectra and avoids significant spectral overlap (Camarero et al., 2002; Cowburn et al., 2004; Xu et al., 1999). To facilitate structural studies of RAGE, we prepared chemically ligated sRAGE, CL-sRAGE, consisting of two segmentally labeled constructs, [U - ^{15}N , ^2H]-VC1-C2 and VC1-[U - ^{15}N]-C2, by using intein-based expressed protein chemical ligation (EPL) (Camarero et al., 2002) (Figure 1A).

The EPL reaction requires a C-terminal thioester group on VC1 and an N-terminal cysteine on the C2 domain (Camarero et al., 2002). The VC1 domain was overexpressed with a C-terminal *Mxe* GyrA intein (Mathys et al., 1999). MESNA (2-mercapto-ethanesulfonic acid) was used to induce intein cleavage, which generated the desired reactive thioester group at the C terminus of the VC1 domain. Mutations 233-VPLE to 233-GCSA were introduced into the linker region, 231–237 (Yatime and Andersen, 2013), between the VC1 and the C2 domains (Figure 1B). The V to G mutation reduces steric hindrance during *trans*-thioesterification and the S-N acyl shift, the PL to CS mutation creates a thrombin recognition sequence (Liu et al., 2008) to facilitate construction of the C2 domain for chemical ligation, and the E to A mutation eliminates the negative charge from glutamate, improving the efficiency of the ligation reaction. Thrombin cleavage of C2 exposes N-terminal cysteine 234. Because the linker is not directly involved in sRAGE dimerization, the mutations should not affect sRAGE dynamics and quaternary structure.

The time course of the EPL reaction was monitored by using SDS-PAGE and western blots (Figures 1C and S1). A new band at ~ 43 kDa, corresponding to CL-sRAGE, gradually appeared and increased in intensity, while the band intensities of both the VC1 and C2 domains at 25 kDa and 15 kDa decreased. The reaction product reached a maximum overnight. Mass spectrometric analysis of CL-sRAGE isolated from polyacrylamide gels (Figure S1) confirmed the authenticity of CL-sRAGE and the presence of the amino acid mutations at the ligation site.

To assess the activity of CL-sRAGE, the binding affinity of a physiological ligand, Ca^{2+} -S100B, was evaluated by using an indirect ELISA (Figure 1D). The dissociation constant of the binding reaction was estimated to be 490 ± 43 nM, which is similar to the value of 500–1,000 nM determined for Ca^{2+} -S100B dimer binding to human sRAGE in vitro (Leclerc et al., 2009), suggesting that CL-sRAGE maintains a native fold and thus can serve as a model to study the structural biology of RAGE.

sRAGE Dimerizes through Both the VC1 and C2 Domains

Chemical shifts and NMR peak intensities of backbone amide protons and nitrogens are exquisitely sensitive to the changes in chemical environment induced by intra- and inter-domain interactions (Cavanagh et al., 2007). The changes in the chemical shifts and NMR peak intensities can be used to identify the inter-molecular interaction surfaces between domains and ambig-

uous distance constraints to generate a model of an sRAGE homo-dimer (de Vries et al., 2010). However, rapid spin-spin relaxation of amide protons in sRAGE dimers hampers NMR analysis and results in broadened signals (Dattilo et al., 2007; Xie et al., 2007). To extend the relaxation time, ^2H was substituted for ^1H in the VC1 domain to dramatically improve the spectral resolution of CL-sRAGE. Chemical shifts of 92% of backbone amide protons and nitrogens of the VC1 and C2 domains were assigned using standard triple-resonance NMR spectra (Cavanagh et al., 2007). Selective ^{15}N labeling of alanine, serine, threonine, lysine, leucine, isoleucine, valine, and phenylalanine was used to assign overlapping residues in the NMR spectra. The solution structure of CL-sRAGE was then studied by separately monitoring two isotopic segmentally labeled domains, [U - ^{15}N , ^2H]-VC1 and [U - ^{15}N]-C2, both free and in CL-sRAGE.

The ^{15}N edited heteronuclear single quantum coherence (^{15}N -HSQC) spectra of free and ligated [U - ^2H , ^{15}N]-VC1 domains exhibited substantial differences in chemical shifts and signal intensities due to ligation with the C2 domain and/or oligomerization of CL-sRAGE. sRAGE exhibits a monomer-dimer equilibrium with a dissociation constant of ~ 100 μM (Sarkany et al., 2011) and also forms higher order oligomers (Xie et al., 2007; Zong et al., 2010). CL-sRAGE spectra were collected at less than 100 μM where the dimer is the predominant oligomer. As a result, each peak in the NMR spectra represents the population average of primarily monomers and dimers in solution, but higher molecular weight oligomers could contribute to changes observed in the chemical shifts and especially in the line shape of the NMR peaks.

Peaks from residues at the dimerization interface exhibit concentration-dependent changes in both chemical shift and signal intensity (Figure 2A, insets). These residues were mapped onto the VC1 domain (Figures 2B and S2A). Residues K110, Y113, R114, and R116 form a contiguous positively charged patch on the V domain, and residues E125, D128, S131, and E132 form a negatively charged patch on the C1 domain (Figure 2B). Another patch is formed by residues L164, E168, and K169 in the C1 domain. Concentration-independent chemical shift and intensity changes in residues G69, G66, G70, W72, S74, L164, K169, G170, V171, E182, F186, M193, V194, and G199 are induced by the ligation of VC1 and C2 domains (Figures 2A and S2A).

Substantial changes in chemical shifts and broadening of intensities are also observed between the free and chemically ligated [U - ^{15}N]-C2 domain (Figures 2C and S2B). Concentration-dependent changes were mapped onto the molecular surface of the C2 domain (Figures 2C, insets, and 2D). A polar patch consisting of residues of Q268, T304, S306, and S307 contributes to the dimer structure of sRAGE. Residues that exhibit concentration-independent changes in chemical shifts and peak intensities, T258, C259, E260, Y299, and S313, are induced by ligation and are likely unrelated to sRAGE dimerization (Figures 2C and S2B).

Mass Spectrometry Provides Distance Constraints within the sRAGE Dimer

To build a reliable model of an sRAGE dimer, ambiguous constraints provided by NMR have to be supplemented by unambiguous distance constraints (de Vries et al., 2010). The

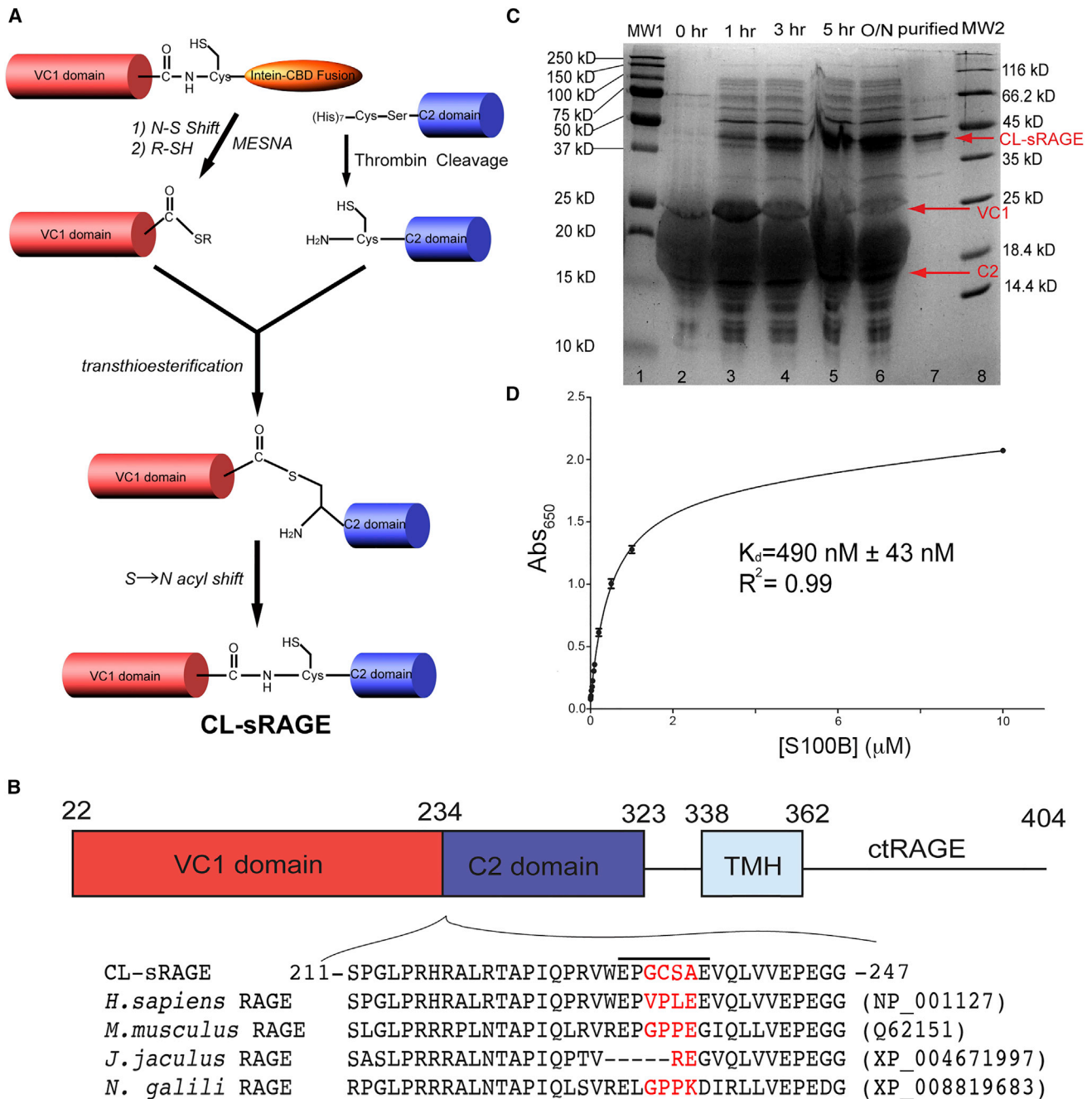


Figure 1. CL-sRAGE Binds to Its Physiological Ligand, Ca^{2+} -S100B

(A) The scheme of chemical ligation. A nucleophilic cysteine thiol group attacks the adjacent carboxyl group, undergoing an N-S shift and is cleaved by 2-mercaptoethane sulfonic acid (MESNA) on the VC1 domain. The C-terminal thioester group of VC1 is free to ligate with the N-terminal cysteine of the C2 domain, released by thrombin cleavage of the His-tag. The subsequent *trans*-thioesterification and S-N acyl shift create a peptide bond.

(B) The ligation site (red) consists of amino acids 233–236 in the linker, indicated by the bar above the sequence, between the VC1 and C2 domains, which is not well conserved across various species.

(C) The generation of chemically ligated sRAGE is monitored through a time course SDS-PAGE experiment. Lanes 1 and 8 are molecular weight markers. Lanes 2–6 are time points collected at 0 hr, 1 hr, 3 hr, 5 hr, and overnight. Lane 7 shows chromatographically purified CL-sRAGE.

(D) ELISA of CL-sRAGE titrated with Ca^{2+} -S100B protein. The data represent three separate experiments.

See also [Figure S1](#).

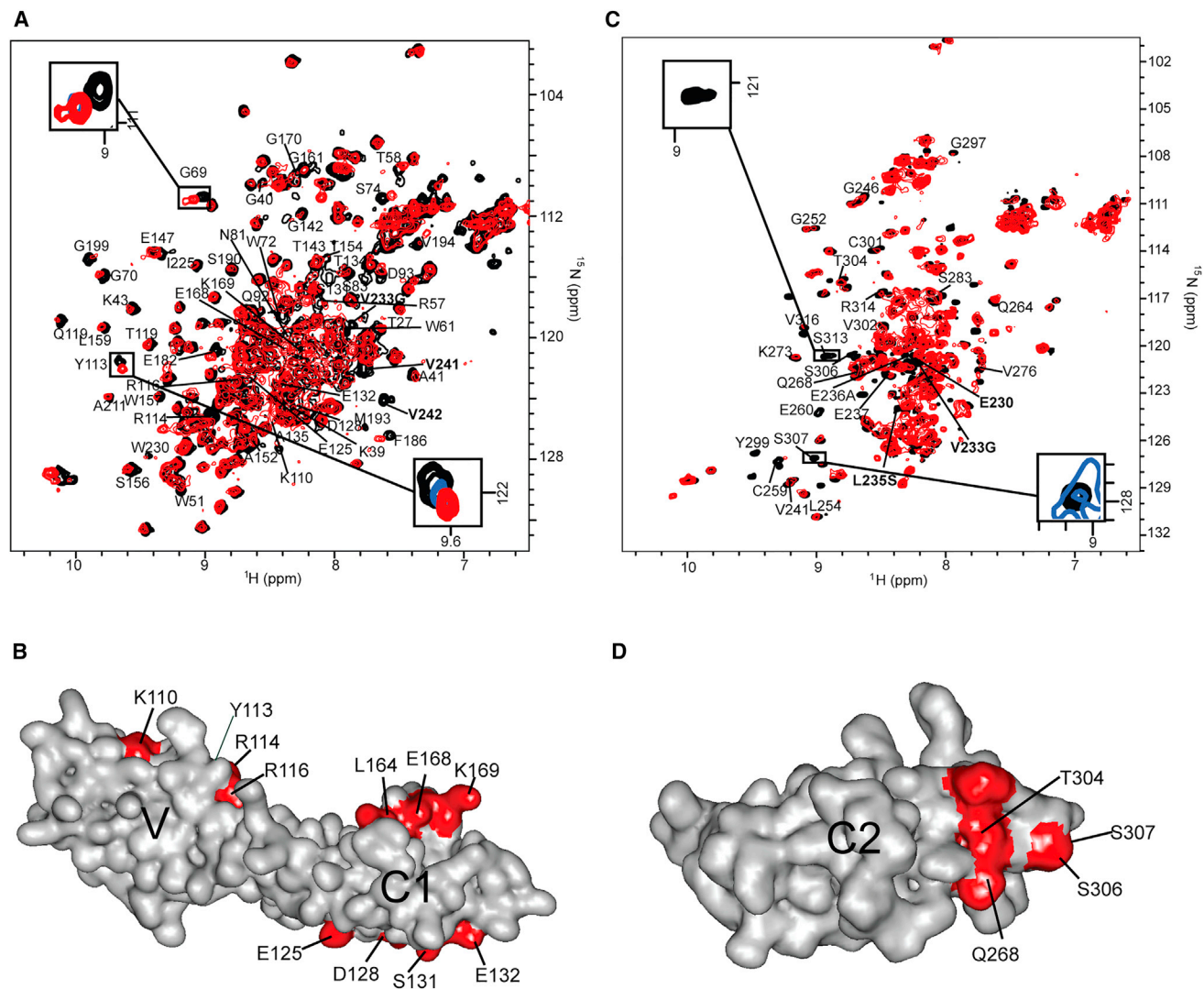


Figure 2. All Three Domains Are Involved in sRAGE Homo-Dimerization

(A) Overlay of the ^{15}N -HSQC spectra of the free $[U\text{-}^2\text{D}, ^{15}\text{N}]$ -VC1 domain (black) and the $[U\text{-}^2\text{D}, ^{15}\text{N}]$ -VC1 domain in CL-sRAGE (red). Y113 and G69 peaks from the free $[U\text{-}^2\text{D}, ^{15}\text{N}]$ -VC1 domain (black) and the $[U\text{-}^2\text{D}, ^{15}\text{N}]$ -VC1 domain in CL-sRAGE at 50 μM (blue) and 80 μM (red) are overlaid in insets. The Y113 peaks exhibit concentration-dependent chemical shift changes consistent with the involvement of this residue in CL-sRAGE dimerization, whereas those of G69 do not.

(B) Inter-molecular interaction surfaces within the homo-dimer (red) are mapped onto the VC1 domain solution structure.

(C) Overlay of the ^{15}N -HSQC spectra of the $[U\text{-}^{15}\text{N}]$ -free C2 domain (black) and the $[U\text{-}^{15}\text{N}]$ -C2 domain in CL-sRAGE (red). S307 and S113 peaks from the free $[U\text{-}^{15}\text{N}]$ -C2 domain (black) and the $[U\text{-}^{15}\text{N}]$ -C2 domain in CL-sRAGE at 40 μM (blue) and 80 μM (red) are overlaid in insets. The S307 peaks exhibit concentration-dependent peak intensity changes consistent with the involvement of this residue in CL-sRAGE dimerization, whereas those of S113 do not. Contour levels in the insert spectra were normalized by a side-chain peak at 8.5 and 111 ppm in proton and nitrogen dimensions, respectively, which exhibited minimal changes in both chemical shift and peak intensity.

(D) Inter-molecular interaction surface within the homo-dimer (red) is mapped onto the C2 domain solution structure.

In (A) and (C), backbone assignments of the residues that exhibited significant changes in chemical shifts and/or peak intensities in CL-sRAGE are labeled. Assignments in bold correspond to residues that were either mutated or become unlabeled due to the molecular constructs used to create CL-sRAGE. See also Figure S2.

combination of chemical cross-linking and mass spectrometric (MS) analysis provided unambiguous distance constraints for the sRAGE dimer. Three chemical cross-linkers, sulfosuccinimidyl 4-(N-maleimidomethyl)cyclohexane-1-carboxylate (sulfo-SMCC), bis-sulfosuccinimidyl suberate (BS_3), and succinimidyl-[(N-maleimidopropionamido)-hexaethyleneglycol] ester ($\text{SM}(\text{PEG})_6$), which span distances of 8.3 \AA , 11.4 \AA , and 32.5 \AA , respectively, were used to probe the architecture of sRAGE.

To minimize artifacts, limited concentrations of cross-linkers were used, resulting in a low (less than 5%) yield of cross-linked products. The shortest probe, sulfo-SMCC, which produces specific amine-to-sulfhydryl conjugates, failed to cross-link sRAGE, thereby placing a lower limit (i.e., 8.3 \AA) on the distance constraints. The sRAGE monomer is elongated, highly positively charged at the V domain, and negatively charged at the C2 domain, and migrates like a 45 kDa protein, which is higher

than its molecular weight of 33 kDa. Multiple bands at ~90 kDa, ~125 kDa, and ~200 kDa appear on SDS-PAGE within 30 min of initiating a cross-linking reaction with BS₃ and SM(PEG)₆ at room temperature, representing sRAGE dimers, trimers, tetramers, and a large oligomer weighing more than 250 kDa (Figure S3). This sequential assembly suggests that, in solution, sRAGE likely possesses more than one oligomerization surface and may not form the simple symmetric dimer proposed by Sarkany et al. (2011) and Sitkiewicz et al. (2013).

Bands isolated from cross-linked dimeric and trimeric CL-sRAGE were proteolyzed in gel using two endoproteinases, trypsin, and Glu-C. The purified peptide mixture was analyzed by using a bottom up proteomics strategy (Chu et al., 2004). An unloaded gel lane and the CL-sRAGE monomer band were also processed by double proteolysis to control against possible false-positives. A representative example of the precursor ion, corresponding to the conjugate of peptide 58–77 with 117–125, which was produced by treatment with BS₃ (Figure 3A) mass spectrometry, is shown (Figure 3B). Overall, four distinctive conjugates were isolated and analyzed by using MS and tandem MS/MS, which placed residue couples K62-K123, K107-K123, and K62-K107 to within 11.4 Å from one another, and K110-C234 within 32.5 Å (Table 1).

sRAGE Is a Non-symmetric Homo-Dimer in Solution

The observation that both the VC1 and C2 domains contribute to sRAGE dimerization is consistent with previous studies of the sRAGE solution structure (Zong et al., 2010; Wei et al., 2012; Su and Berger, 2012). To generate a structural model of an sRAGE homo-dimer, the HADDOCK program (de Vries et al., 2010; Wassenaar et al., 2012) was used to dock two sRAGE monomers (Yatime and Andersen, 2013) by using both the ambiguous distance constraints derived from the inter-molecular interaction surfaces between domains (Figures 2B and 2D) and the unambiguous distance constraints defined by cross-linking (Figure 3, Tables 1 and S1).

The linker between the C1 and C2 domain (Figure 1B), consisting of five residues (231–237) (Yatime and Andersen, 2013), was assigned to be semi-flexible. NMR and cross-linking-derived distance constraints were consistent with one structural family of sRAGE. The best-refined cluster has an interface root-mean-square deviation (RMSD) of 2.7 Å, a cluster size of 200, and inter-molecular energy equal to -87.6 ± 1.5 kcal mol⁻¹ (Table S2). The sRAGE homo-dimer interface consists of a total buried surface area of 1443 ± 64 Å² and involves regions of both the VC1 and C2 domains (Figure 4). Importantly, because the C1-C2 linker (Figure 1B) is not involved in dimerization, the HADDOCK structure calculated for the CL-sRAGE dimer should be compatible with that of wild-type sRAGE.

The principal sRAGE homo-dimer inter-molecular interactions occur between the G strand of the V domain and the A strand of the C1 domain, as well as between the CD loop of the C1 domain and the FG loop of the C2 domain (Figure 4A). Key interaction surfaces involve electrostatic contacts, K110-E125 and R114-D128, between the V and C1 domains, and electrostatic contact K169-Q268 and potential hydrogen bonds between residues R116-S131, L164-S306, and E168-T304 between the C1 and C2 domains (Figure 4B). All unambiguous constraints are satisfied within 0.2 Å (Figures 4A and 4B, top

panels). The molecular surfaces of the asymmetric sRAGE homo-dimer consist of two parallel J-shaped monomers oriented head to head (Figure 4C). The structure suggests that the oligomers larger than dimers can form by utilizing the same interaction surfaces (Figure 4C).

Electrostatic surface potentials mapped onto a molecular representation of the sRAGE homo-dimer shows electrostatic compensation between the positively charged V domain and the negatively charged C2 domain that minimizes electrostatic repulsion between the two generally positive-charged VC1 domains (Figure 4C). When in contact with the VC1 domain, the C2 domain is directed toward the cell membrane. A distance of approximately 50 Å is observed between the last proline residue on the G strand of the C2 domain of one monomer and the corresponding residue of the cognate monomer within an sRAGE homo-dimer. This orientation defines the molecular dimension of the cytosolic domain of the homo-dimer (Figure 1B). It is likely that the relative distances between the C termini of sRAGE are important for signal transduction because the C2 domain connects directly to the transmembrane helix and the cytosolic tail.

¹⁵N-NMR relaxation rates are very sensitive to monomer-dimer equilibria as they strongly depend on the rotational correlation time of the dimer in solution and can provide independent confirmation of the validity of models of interacting proteins (Fushman, 2012). HydroNMR (Bernado et al., 2002; Blobel et al., 2009; Garcia de la Torre et al., 2000) was used to compute theoretical relaxation data for the monomer and the HADDOCK (de Vries et al., 2010; Wassenaar et al., 2012) model of the dimer. A dimerization constant, K_d , was calculated by fitting theoretical relaxation data to experimental values (Figure S4). This approach gave a well-defined minimum, $\chi^2 = 1.025$, corresponding to a K_d of 120 ± 12 μM, in good agreement with previous estimates of the monomer-dimer equilibrium constant (Sarkany et al., 2011). The ability to predict the expected relaxation rates of macromolecules of known structure opens the way to sensitive and structurally informative methods to characterize weakly interacting protein-protein complexes.

S100B Binding Defines the Geometry of Oligomeric RAGE

Ca²⁺-S100B is a physiological ligand of RAGE that initiates RAGE-dependent signal transduction (Hofmann et al., 1999; Koch et al., 2010). Changes in the ¹⁵N-HSQC NMR spectra of [^U-¹⁵N]-S100B with and without CL-sRAGE, and of [^U-²H, ¹⁵N]-VC1 in CL-sRAGE with and without Ca²⁺-S100B, were used to define the interaction surfaces between the VC1 domain and dimeric Ca²⁺-S100B (Figure S5). Mapping these changes onto the VC1 domain reveals positively charged residues at opposite ends of the interacting surface on the V domain, K43, K44, A101, M102, N103, R104, N105, G106, and K107 (Figure 5A). Mapping the interaction surface residues of S100B, F43, L44, E45, E49, A78, M79, V80, T81, T82, A83, H85, E86, F87, F88, E89, and H90 shows negatively charged residues at opposite ends of a hydrophobic pocket (Figure 5B). These results are consistent with the NMR studies of the Ca²⁺-S100B binding to isolated VC1 (Koch et al., 2010).

Changes in the peak intensities of VC1 domain residues K39, A41, R48, W61, V63, R98, E125, G125, A152, T154, V165, R169,

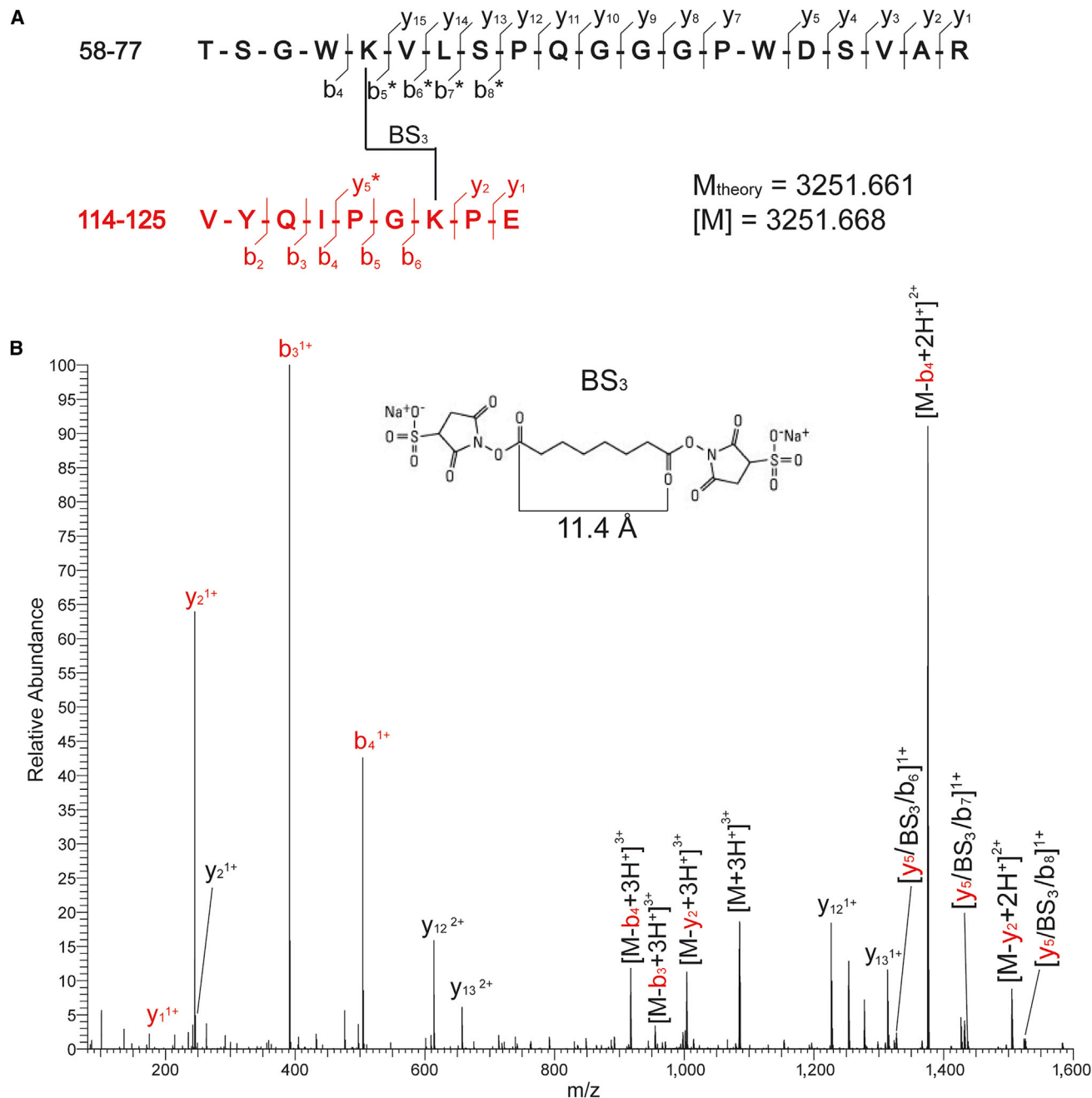


Figure 3. MS Characterization of Cross-Linked Peptides from CL-sRAGE

(A) Sequence and composition of cross-linked peptides. Observed fragment ions and their charge states are labeled according to standard nomenclature. BS₃-modified fragments are labeled with stars (*).

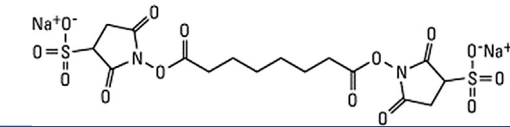
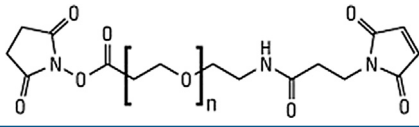
(B) A representative high-energy collision (HCD) spectrum obtained upon activation of the cross-linked product observed at m/z 1,084.895 in the digestion mixture. The experimental mass (M) afforded by this triply charged precursor ion matched the theoretical mass of 3,251.661 calculated from the putative elemental composition. Black and red colors represent the cross-linked peptides. The observed fragment ions (y and b fragment ions) afforded almost complete coverage, which revealed the presence and position of the BS₃ moiety within the cross-linked product.

See also Figure S3.

V171, T195, A197, and V233, and of S100B residues L27, R29, E46, I47, A75, F76, and C84, do not form a contiguous interaction surface, and likely represent indirect changes within CL-sRAGE and S100B upon forming the complex (Figure S5).

Only slight changes arise between the ¹⁵N-HSQC spectra of [*U*-¹⁵N]-C2 in CL-sRAGE with and without Ca²⁺-S100B, implying no significant alteration of the C2 domain conformation within CL-sRAGE upon Ca²⁺-S100B binding.

Table 1. Cross-Linker Reagents and Cross-Linked Peptides and Residues

	BS ₃			SM(PEG) ₆
Cross-linker reagent				
Spacer length	11.4 Å			32.5 Å
Specificity	homobifunctional reactive toward primary amides			heterobifunctional thio-ether bond formation between primary amide and cysteine sulfhydryl group
Cross-linked RAGE sequence	T58-R77 to V117-E125	N105-E108 to V117-E125	T58-R77 to V117-E125	E108-R114 to V229-E237
Cross-linked residues	K62-K123	K107-K123	K62-K107	K110-C234
Intra-/inter-molecular	inter-molecular	inter-molecular	intra-molecular	inter-molecular
M _{theoretical}	3,251.661	1,613.829	2,668.319	2,359.052
M _{experimental}	3,251.668	1,613.834	2,668.329	2,359.056
Error	-2 ppm	-3.1 ppm	-3.8 ppm	1.7 ppm

By using the amine-to-amine cross-linker BS₃ to determine if CL-sRAGE oligomerization is induced by Ca²⁺-S100B, a species slightly smaller than 75 kDa, which is absent in cross-linked CL-sRAGE oligomers, was observed (Figure S6). The size is consistent with a combination of a 45 kDa CL-sRAGE monomer and a 20 kDa Ca²⁺-S100B dimer. MS and tandem MS/MS analysis revealed that the cross-linked complex involves CL-sRAGE sequence 114–125 and S100B sequence 48–52, providing an unambiguous distance constraint for structure calculations (Figure S6 and Table S1).

HADDOCK modeling of the Ca²⁺-S100B-sRAGE complex based on the unambiguous and ambiguous distance constraints is shown in Figure 5C. Ca²⁺-S100B dimers bind to two V domains from different sRAGE homo-dimers. The model of the sRAGE homo-dimer (Figure 4) was used in the docking. The best-refined cluster has an interface RMSD of 6 Å, a cluster size of 196, and inter-molecular energy equal to -133 ± 3 kcal mol⁻¹ (Table S2). Binding of the Ca²⁺-S100B dimer co-localizes two sRAGE homo-dimers but does not disrupt the individual sRAGE homo-dimer structure. No additional interactions between the two homo-dimers were identified.

Ca²⁺-S100B-induced oligomerization of sRAGE homo-dimers results in a distance between the C termini of C2 domains located on each sRAGE homo-dimer of ~ 100 Å. This increased molecular dimension of the cytosolic components of oligomerized RAGE compared with free RAGE homo-dimers (~ 50 Å) is comparable with the spacing between the FH1 domains of the DIAPH1 dimer (Figure 5C). Free DIAPH1 is a dimer that binds to ctRAGE (Rai et al., 2012a) and is required for ligand-induced RAGE signal transduction (Bianchi et al., 2011; Hudson et al., 2008; Toure et al., 2012).

Free DIAPH1 is maintained in a compact state through an intra-molecular interaction between the N-terminal diaphanous autoregulatory domain and the C-terminal diaphanous inhibitory domain (Figure 6A, left panel). In this configuration, the two FH1 domains of the DIAPH1 dimer, which are the binding sites for RAGE (Hudson et al., 2008; Rai et al., 2012a), are spaced ~ 100 Å from each other (Maiti et al., 2012; Shimada et al.,

2004), closely matching the distance between the C termini of RAGE homo-dimers ligated with S100B. Thus, the structural model suggests a mechanism for signal transduction in which Ca²⁺-S100B dimer binding may promote oligomerization of RAGE homo-dimers, facilitating clustering on the cell surface, recruitment of DIAPH1, and subsequent signal transduction.

Ligand-Induced RAGE Oligomerization Activates DIAPH1-Dependent Signal Transduction

To test the assumptions of the structural model, fluorescence microscopy and cell signaling experiments were used to probe the in-cell interaction of full-length RAGE with its effector DIAPH1. Two plasmids expressing full-length RAGE fused with YFP, and full-length DIAPH1 fused with CFP were individually transfected into HEK293 cells. As expected, RAGE-YFP was localized onto the plasma membrane, and DIAPH1-CFP exhibited a cytosolic distribution. Transfecting both plasmids into HEK293 cells led to co-localization of the two proteins (Figure 6B, upper panels).

RAGE-DIAPH1 co-localization was quantitatively described by using a normalized mean deviation product (nMDP), which ranges from -1 for negative correlation (exclusion) between the positions of two fluorescently labeled proteins to +1 for positive correlation (co-localization). Under our experimental conditions, the average nMDP value for RAGE-YFP and DIAPH1-CFP was 0.055 ± 0.003 . The nMDP increased to 0.065 ± 0.003 ($p < 0.05$) upon adding Ca²⁺-S100B (Figure 6B, lower panels). This small but statistically significant increase is consistent with ligand-induced DIAPH1 binding to RAGE.

The deletion mutant of DIAPH1, Δ DAD-DIAPH1, exists in an extended conformation in which the FH1 domains can be within ~ 50 Å of each other (Maiti et al., 2012) (Figure 6A, right panel). This distance closely matches the distance between the C termini in free sRAGE homo-dimers (Figure 4C) and suggests that under physiological conditions, Δ DAD-DIAPH1 may strongly bind to RAGE (Rai et al., 2012a). Indeed, Δ DAD-DIAPH1 readily co-localizes with RAGE as indicated by an nMDP of 0.091 ± 0.001 (Figure S7). This value is 40% greater than the

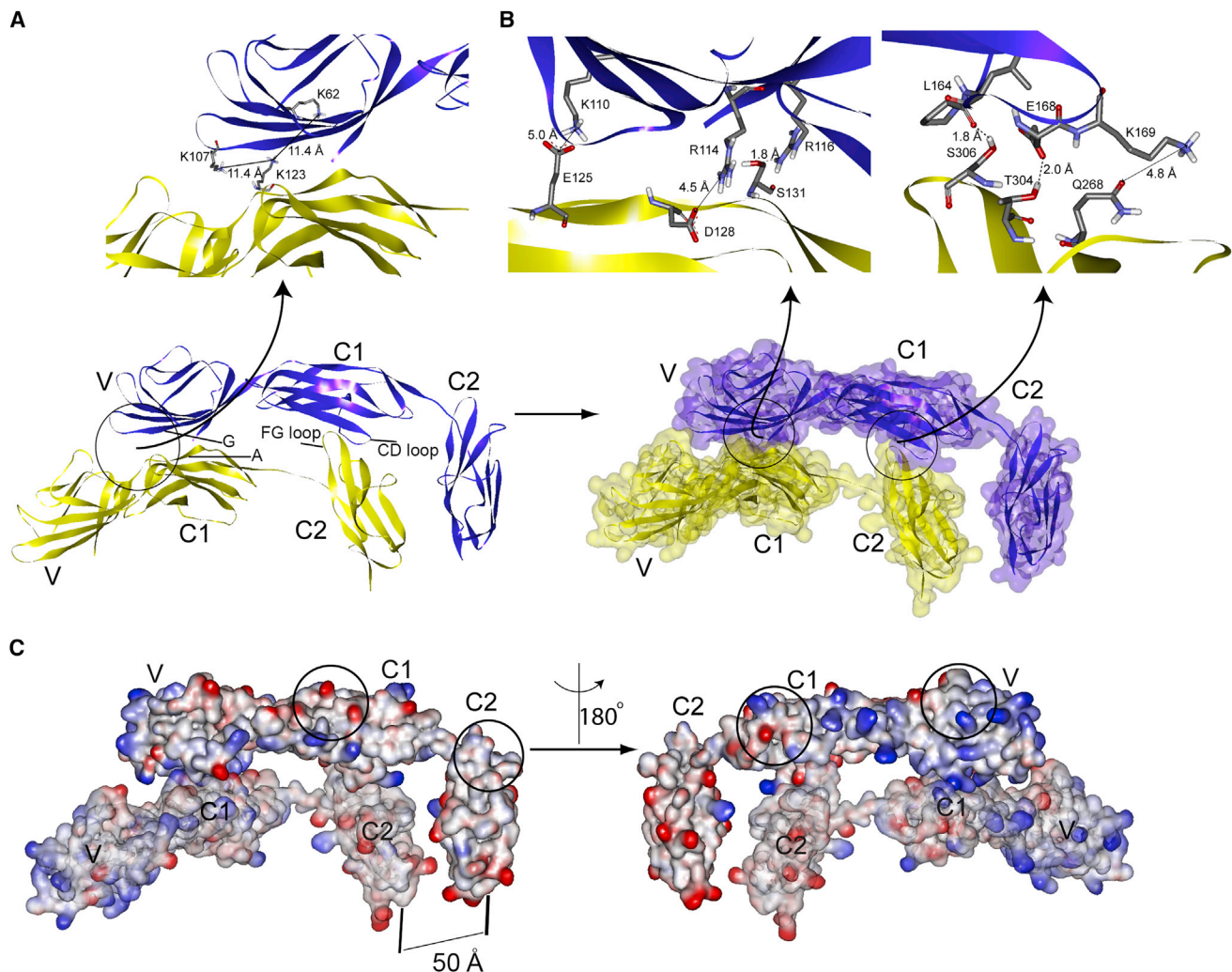


Figure 4. Model of the sRAGE Homo-Dimer

(A) Two monomers (purple and yellow) orient head to head with each other in the flat ribbon display. The elements of the sRAGE secondary structure involved in dimerization are labeled based on the VC1 (Koch et al., 2010) and C2 (Yatime and Andersen, 2013) secondary structure assignments. A close up of two unambiguous distance constraints is shown in the upper panel. The distances between cross-linked residues, K62-K123 and K107-K123, match the BS₃ spacer length.

(B) A half-transparent molecular surface and flat ribbon display of the homo-dimer model is shown in two colors. Electrostatic contacts are observed between residues K110-E125, R114-D128, and K169-Q268, while hydrogen bonds are observed between residues R116-S131, L164-S306, and E168-T304 (upper panel).

(C) The electrostatic potential mapped onto the solution structure of the sRAGE homo-dimer reveals a global interaction between the monomers: The electrostatic surface potential of the VC1 domain is positive (blue), and that of the C2 domain is generally negative (red). The localization of opposite charge clusters facilitates charge neutralization and depolarization in the homo-dimer. Higher order sRAGE oligomers can form by utilizing solvent-exposed dimerization surfaces (circled regions).

See also Figure S4, Tables S1 and S2.

value obtained for RAGE-full-length DIAPH1 co-localization. In the presence of Ca²⁺-S100B, co-localization increases further to nMDP = 0.097 ± 0.003, p < 0.05 (Figure 6C).

The strong co-localization of RAGE-YFP and ΔDAD-DIAPH1-CFP allowed the use of Förster resonance transfer experiments (FRET) to assess the likelihood of a binding interaction (<50 Å) between fluorescently labeled RAGE-YFP and ΔDAD-DIAPH1-CFP. An 8% ± 2% (Figure S7) and 10% ± 3% (Figure 6C) increase in donor (RAGE-YFP0 emission due to acceptor (ΔDAD-DIAPH1-CFP) photobleaching were observed without and with the addition of Ca²⁺-S100B, respectively, suggesting

that ΔDAD-DIAPH1 interacts with RAGE in the absence of RAGE ligands and therefore may serve as an effector for RAGE signaling.

Wild-type (WT) and DIAPH1 knockout smooth muscle cells (KO SMCs) were used to assess the effect of ligand-dependent RAGE oligomerization on RAGE signaling. The cells, which constitutively express RAGE, were transfected with an empty vector, full-length DIAPH1-CFP, or ΔDAD-DIAPH1-CFP (Figure 6D). Phosphorylation of AKT kinase was used as a probe of Ca²⁺-S100B-dependent RAGE activation (Rai et al., 2012a) (Figures 6D and 6E).

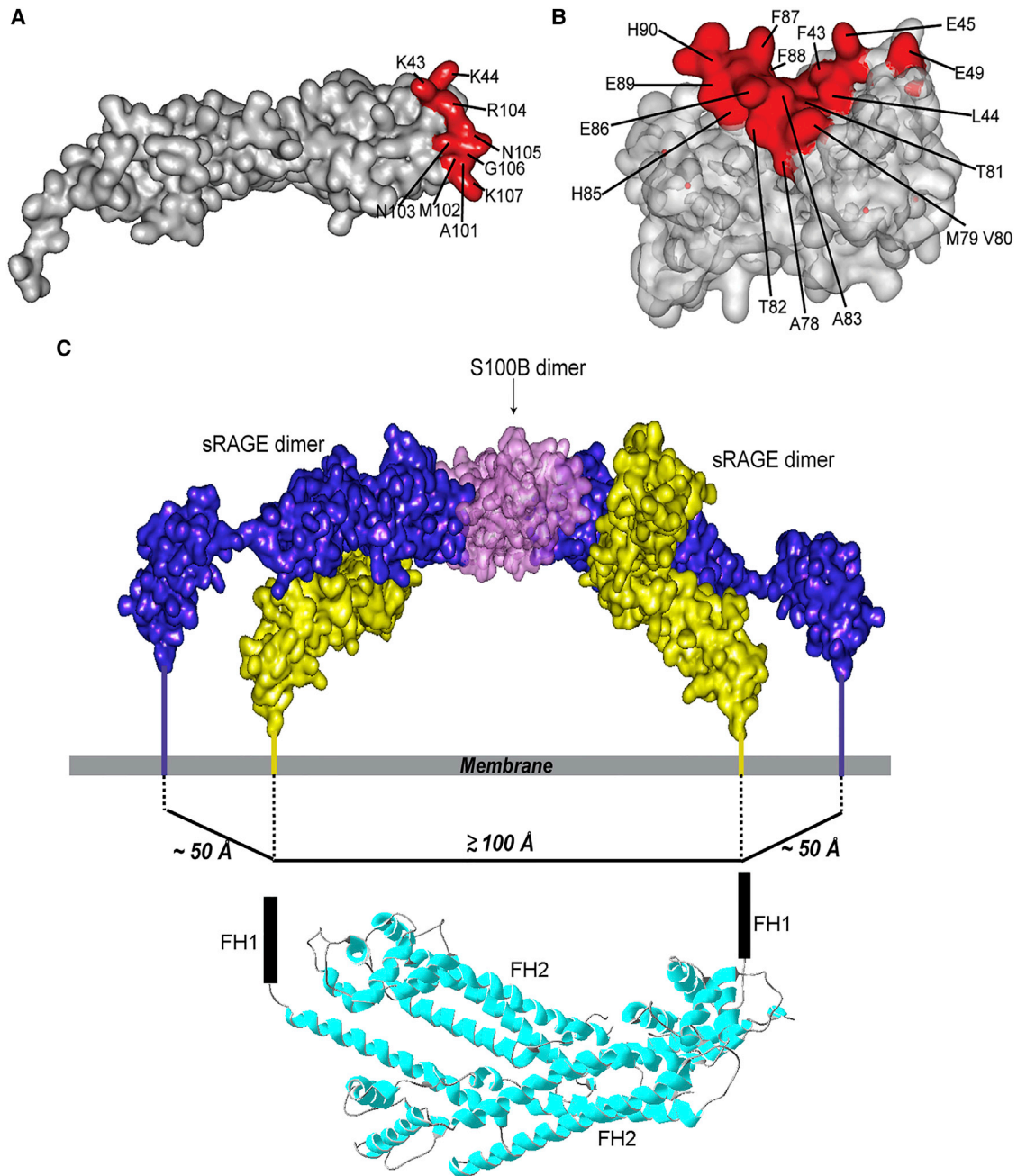


Figure 5. S100B Induced Homo-Dimer Clustering and a Dramatic Increase in RAGE Dimensions

(A) V domain residues that comprise the VC1-Ca²⁺-S100B intermolecular interaction surface (red) mapped onto the VC1 domain.

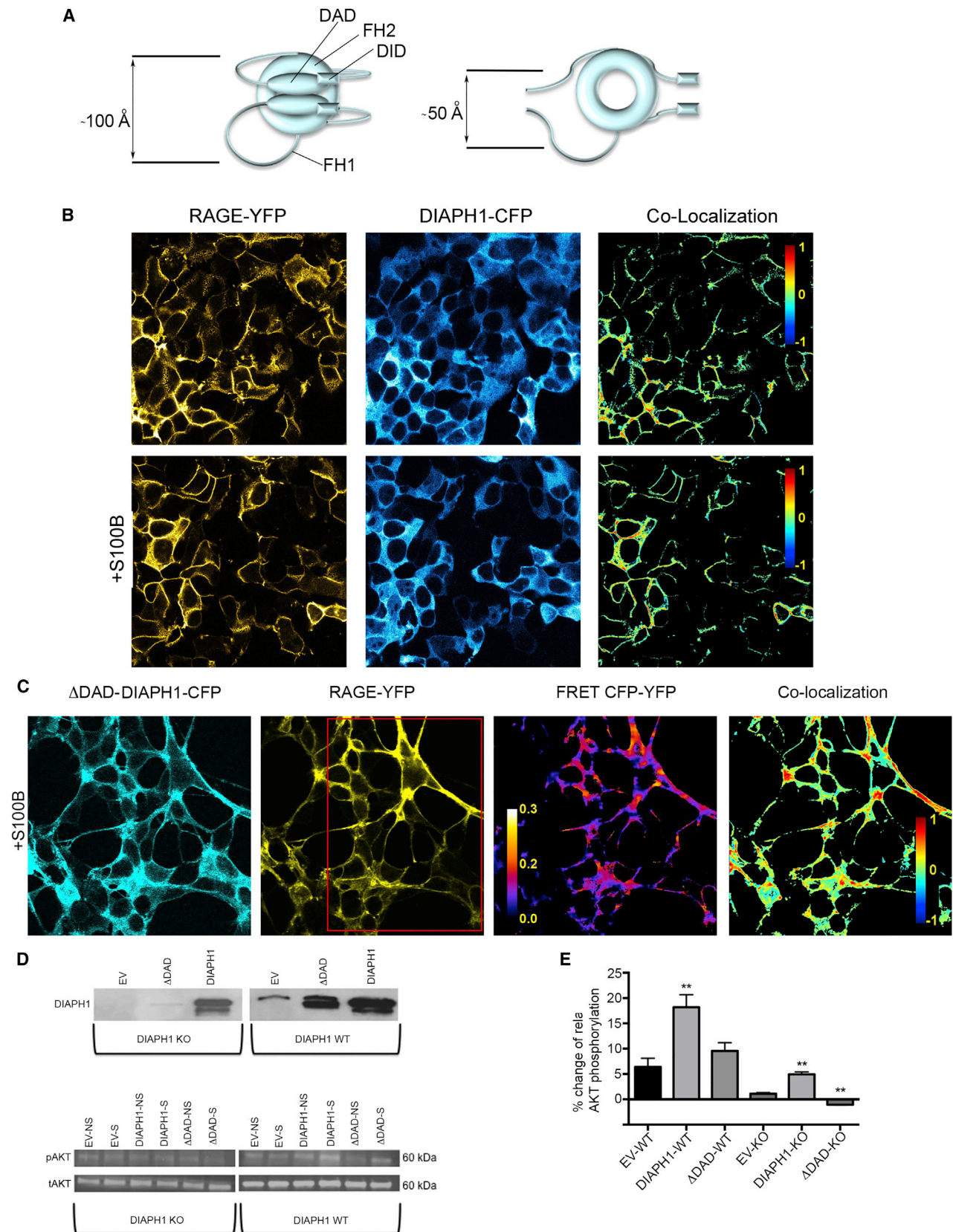
(B) Ca²⁺-S100B residues that comprise the VC1-Ca²⁺-S100B intermolecular interaction surface (red) mapped onto the Ca²⁺-S100B dimer.

(C) Model of an Ca²⁺-S100B dimer bound to two sRAGE homo-dimers showing the proposed transmembrane interaction between RAGE and DIAPH1. The spacing between the ctRAGE-binding FH1 domains of the DIAPH1 dimer (PDB: 1V9D (Shimada et al., 2004)) is comparable with the distance between the C termini of the two homo-dimers.

See also Figures S5 and S6; Tables S1 and S2.

Basal RAGE activation, observed in WT SMCs transfected with empty vector, is in response to endogenous DIAPH1 (Figures 6D and 6E). No activation was observed in the DIAPH1 KO SMCs transfected with empty vector (Hudson et al., 2008; Rai et al., 2012a; Toure et al., 2012) as expected, since DIAPH1 is necessary for Ca²⁺-S100B-dependent RAGE activation (Fig-

ures 6D and 6E). Transfecting WT and KO SMCs with DIAPH1 led to statistically significant 20% and 5% increases in AKT phosphorylation, implying that the presence of full-length DIAPH1 is required for RAGE signaling. Transfecting ΔDAD-DIAPH1 into WT SMCs resulted in a statistically insignificant increase in AKT phosphorylation, and a decrease in KO SMCs,



(legend on next page)

implying that Δ DAD-DIAPH1 does not facilitate ligand-dependent RAGE signaling. Thus, in accordance with the proposed structural mechanism for signal transduction, Ca^{2+} -S100B-induced oligomerization of RAGE on the surface of the cell membrane leads to increased DIAPH1 binding, which in turn induces phosphorylation of the intracellular RAGE effector serine/threonine cAMP-dependent protein kinase A, AKT (Rai et al., 2012a).

DISCUSSION

Homo-dimerization is essential for RAGE-mediated signal transduction (Wei et al., 2012; Zong et al., 2010). Due to weak interactions between sRAGE monomers, the crystal structures of sRAGE (Yatime and Andersen, 2013) or its isolated domains (Koch et al., 2010; Park et al., 2010) do not clearly reveal the oligomerization surfaces that are important for the RAGE resting state or ligand-dependent RAGE self-association required for signal transduction (Schmidt et al., 2001; Zong et al., 2010). The four existing crystal structures indicate two different dimerization surfaces deduced from crystal packing (Koch et al., 2010; Park et al., 2010; Xu et al., 2013; Yatime and Andersen, 2013) and place highly positively charged V domains in immediate proximity to each other, which is unlikely to occur in solution but could be stabilized by the interaction with negatively charged heparin (Xu et al., 2013), a known inhibitor of RAGE signaling (Rao et al., 2010). The complete structure of full-length RAGE or extracellular sRAGE in solution is difficult to determine by using NMR spectroscopy due to its large size. To resolve the oligomeric solution structure of free sRAGE and in complex with the physiological ligand Ca^{2+} -S100B, we employed a hybrid method combining analysis of segmentally labeled sRAGE with high-resolution NMR and cross-linking with MS detection.

sRAGE was constructed from two independent segmentally labeled units, the VC1 and C2 domains. NMR spectroscopy was used to identify the intra- and inter-molecular interaction surfaces between these domains. These surfaces were converted into ambiguous constraints for protein docking analysis. Unambiguous distance constraints were obtained from cross-linking followed by protease digestion and MS analysis. There was agreement between the ambiguous constraints derived

from NMR and unambiguous constraints derived from chemical probing. The combination of isotopic segmental labeling together with NMR analysis and protein chemical cross-linking represents a very effective novel technique for analyzing structures of weakly oligomerizing proteins (Fabris and Yu, 2010; Friedhoff, 2005; Trakselis et al., 2005).

A structural model resolving the interaction surfaces and orientation of each monomer within the sRAGE homo-dimer was described. The model suggests how sRAGE oligomers larger than dimers, which are implicated in ligand-independent RAGE signaling in RAGE overexpressing melanoma cells (Megh-nani et al., 2014), can form. The negatively charged C2 domain stabilizes the sRAGE homo-dimer structure by interacting with the positively charged VC1 domain, underscoring the importance of the VC1 and C2 domains for homo-dimerization (Reverdatto et al., 2013; Sitkiewicz et al., 2013; Wei et al., 2012; Zong et al., 2010). Indeed, VC1 domain residues K110, R114, R116, E125, D128, and S131, involved in homo-dimerization, match those identified by cross-linking probes as being protected from deuterium exchange (Sitkiewicz et al., 2013). In addition, C2 domain residue S307, which is involved in homo-dimerization, is one of the residues implicated in binding a peptide aptamer that inhibits ligand-induced RAGE signaling (Reverdatto et al., 2013).

A structural model of Ca^{2+} -S100B binding to sRAGE was also developed and a mechanism for Ca^{2+} -S100B-dependent RAGE signaling was proposed and tested. The Ca^{2+} -S100B binding and homo-dimerization sites on sRAGE are distinct, permitting a higher order oligomer to assemble (Figures 4 and 5). FRET analysis of unstimulated oligomeric RAGE indicates that the intracellular C termini are located within 50 Å (Xie et al., 2008), consistent with the model of the homo-dimer (Figure 4). Ca^{2+} -S100B binding induces RAGE oligomerization and increases the distance between the C termini to 100 Å (Figure 5), closely matching the distance between the FH1 binding domains of the intracellular effector DIAPH1 (Maiti et al., 2012), which is required to establish strong Ca^{2+} -S100B-dependent RAGE signaling (Hudson et al., 2008; Toure et al., 2012) (Figure 6).

The mechanism proposed for S100B-induced RAGE signal transduction is consistent with experimental observations showing that RAGE forms constitutive multimers (Wei et al.,

Figure 6. Full-Length DIAPH1 Is Required for RAGE Signaling

(A) Schematic representation of free full-length DIAPH1 (left) and Δ DAD-DIAPH1 (right). The compact conformation of free full-length DIAPH1 FH2 domains form a lasso orienting the FH1 domains \sim 100 Å apart (Maiti et al., 2012; Shimada et al., 2004). The extended conformation of Δ DAD-DIAPH1 allows the FH1 domains to span a smaller distance of \sim 50 Å.

(B) RAGE-YFP and DIAPH1-CFP co-localize on the HEK293 cell surface (upper panels). Adding Ca^{2+} -S100B (lower panels) further increases the co-localization from $n\text{MDP} = 0.055 \pm 0.003$ to $n\text{MDP} = 0.065 \pm 0.003$, $p < 0.05$.

(C) Δ DAD-DIAPH1-CFP and RAGE-YFP readily co-localize on HEK293 cells after adding Ca^{2+} -S100B. FRET between CFP and YFP was observed after photobleaching RAGE-YFP in the region shown by the red rectangle. The FRET efficiency between RAGE-YFP and Δ DAD-DIAPH1-CFP was $10\% \pm 3\%$, whereas acceptor photobleaching typically results in over a 90% decrease in fluorescence.

(D) Full-length DIAPH1 supports RAGE signaling, whereas Δ DAD-DIAPH1 does not. WT SMCs (right panels) and DIAPH1 KO SMCs (left panels) transfected with either empty vector (EV), Δ DAD-DIAPH1-CFP (Δ DAD), or DIAPH1-CFP (DIAPH1) were stimulated with $1 \mu\text{M}$ Ca^{2+} -S100B. Cell lysates were separated by SDS-PAGE and immunoblotted with antibodies specific for DIAPH1 (upper panels), phospho-AKT (middle panels), or total AKT (bottom panels). NS and S stand for non-stimulated and stimulated cells.

(E) Changes in phosphorylation levels of AKT following stimulation by Ca^{2+} -S100B. Double asterisks at the top of the bars represent a statistically significant ($p < 0.05$) change in AKT phosphorylation due to stimulation compared with EV. Note the apparent lack of RAGE signaling stimulation when SMCs are transfected with either empty vector or Δ DAD-DIAPH1-CFP. NS and S stand for non-stimulated and stimulated cells. The data represent three separate experiments. See also Figure S7.

2012; Xie et al., 2007, 2008; Zong et al., 2010). These multimers are stabilized by both the weakly dimerizing extracellular domains, as exhibited by sRAGE, and oligomerization of cytosolic RAGE (ctRAGE) (Su and Berger, 2012). Ca²⁺-S100B binding to RAGE shifts the equilibrium distribution toward higher order oligomeric states without causing a major conformational change (Choudhuri et al., 2005; Metzger, 1992). Subsequent binding of DIAPH1 results in signal transduction. Importantly, site-specific peptide aptamers have been identified that bind to individual V, C1, and C2 domains of RAGE and inhibit S100B-dependent RAGE signal transduction (Reverdatto et al., 2013). The use of peptide aptamers selected to inhibit RAGE homo-dimerization and/or oligomerization may prove to be a viable therapeutic strategy to control RAGE-mediated potentiation of cell transformations into pathological states.

EXPERIMENTAL PROCEDURES

Chemical Ligation: Expressed Protein Ligation

The N-terminal His-tag of the C2 domain was cleaved by thrombin (Novagen) at 37°C for 2 hr before being chemically ligated with the VC1 domain. The two protein domains were mixed in native buffer, 20 mM sodium phosphate (pH 7.2), 500 mM NaCl, containing 50 mM MESNA, 1 mM EDTA, and 4-(2-aminoethyl) benzenesulfonyl fluoride hydrochloride (AEBSF) at room temperature for 16 hr. The chemically ligated sRAGE was dialyzed into 20 mM sodium phosphate buffer (pH 6.0), 100 mM Na₂SO₄, loaded onto a HiTrap SP-FF affinity chromatography column (GE Healthcare) and eluted with a gradient of Na₂SO₄ from 100 mM to 500 mM. Fractions containing the eluted protein were dialyzed into 20 mM sodium phosphate (pH 7.5) and loaded onto a HiTrap Q-FF affinity chromatography column. The protein was eluted with a gradient of Na₂SO₄ from 0 mM to 150 mM prior to gel-filtration chromatography on an analytical SE-75 column (Amersham Biosciences). Purity was estimated to be >80% by Coomassie-stained SDS-PAGE.

Cross-Linking Reaction

Cross-linking was performed by using a homo-bifunctional (amine-to-amine) cross-linker BS₃, which forms an 11.4 Å stable conjugate between amino groups, and hetero-bifunctional (amine-to-sulphydryl) cross-linkers, sulfo-SMCC with a spacer arm of 8.3 Å and SM(PEG)₆ with a spacer arm of 32.5 Å (Table 1).

Sulfo-SMCC (10 mM) or 100 mM BS₃ in 20 mM sodium phosphate (pH 7.2), 50 mM Na₂SO₄, was added to ~50 μM purified CL-sRAGE in the same buffer to final concentrations of 1, 2.5, and 5 mM, which are 20-, 50-, and 100-fold molar excess over the protein. The reaction mixture was incubated at room temperature for 30 min or on ice for 2 hr. After 5, 15, 30, 60, and 120 min, 200 μL aliquots were taken from the reaction mixtures and NH₄HCO₃ was added to a final concentration of 20 mM to quench the reactions.

SM(PEG)₆ was dissolved in dry DMSO at 250 mM and added to the CL-sRAGE solution to a final concentration of 1 mM. The reaction mixture was incubated either at room temperature for 30 min, or on ice for 2 hr and quenched as above.

Mass Spectrometry

Cross-linked peptides in 1% acetic acid were desalted before MS analysis. Typically, 5–10 μL aliquots were loaded onto a 250 μm silica column packed with 10 μm, 300 Å stationary phase Jupiter C18 resin. Peptides were washed with 200 μL of 1% acetic acid and eluted with 10–30 μL of 70% acetonitrile and 1% acetic acid. Peptide samples (3–6 μL) were loaded into quartz emitters and characterized by electrospray ionization-mass spectrometry using a Thermo Scientific Orbitrap Velos mass spectrometer. The emitter voltage was held at 0.8–1.2 kV and the ion transfer tube temperature was 200°C. Full scans were acquired between 300 and 2,000 m/z with a mass resolution in excess of 100,000. Putative cross-linked species were fragmented in the collision cell with 20 eV–50 eV of energy. Tandem mass spectra were acquired in the Orbitrap mass analyzer over a range of 80–2000 m/z with a mass reso-

lution in excess of 100,000. Experimental data were analyzed manually using the MSX-3D software package (Heymann et al., 2008).

Docking Studies

HADDOCK (de Vries et al., 2010; Wassenaar et al., 2012) was used to dock two sRAGE monomers to form an sRAGE homo-dimer, and to dock sRAGE monomers and Ca²⁺-S100B to form the sRAGE-Ca²⁺-S100B complex by using the previously determined structures of RAGE-VC1C2 (PDB: 4LP5; Yatime and Andersen, 2013) and Ca²⁺-S100B (PDB: 2H61; Ostendorp et al., 2007). Positive and negative cross-link lengths were used to define unambiguous intermolecular distance constraints. Chemical shift perturbations observed upon complex formation were used to define ambiguous interaction constraints for residues at the interface (Table S1). Active residues were defined as those having either chemical shifts changes larger than 0.25 ppm or peak broadening greater than 80% compared with free protein. Passive residues were defined as all of the residues surrounding the interaction surfaces. A total of 5,000 rigid-body docking trials were carried out using the standard HADDOCK protocol. The 100 lowest-energy solutions were used for subsequent semi-flexible simulated annealing and water refinement. The five lowest-energy structures were used to represent the complex (Table S2). Validation of the structures was performed with PROCHECK (Laskowski et al., 1993).

NMR Spectroscopy

Standard double- and triple-resonance spectra ¹⁵N-HSQC, HN(CA)CO, HNCO, HN(CO)CA, HNCA, CBCA(CO)NH, and HNCACB (Cavanagh et al., 2007) were acquired at 298 K using an Avance Bruker spectrometer operating at a ¹H frequency of 700 MHz and equipped with a single z axis gradient cryoprobe. ¹⁵N-HSQC spectra of [¹⁵N]-alanine, -serine, -threonine, -valine, -leucine, -lysine, -isoleucine, -phenylalanine, and -tryptophan labeled free VC1 domain were acquired to help assign chemical shifts. ¹⁵N longitudinal (R₁) and transverse (R₂) relaxation rates were measured by using 2D ¹H-¹⁵N correlation pulse sequences (Cavanagh et al., 2007). For the R₁ and R₂ experiments, 16 and 24 scans, respectively, were collected per t₁ point. The ¹⁵N R₁ and R₂ values were obtained using eight delays, 40, 60, 140, 240, 360, 520, 720, and 1,200 ms, for the R₁ experiments and 16.2, 32.4, 48.6, 64.8, 81, 97.2, 113.4, and 129.6 ms for the R₂ experiments. All spectra were processed using TOPSPIN 2.1 (Bruker), and assignments were made using CARA (Masse and Keller, 2005).

We first attempted to use paramagnetic relaxation enhancement (PRE) of the NMR signal (Tang et al., 2008; Tzeng et al., 2012) to derive unambiguous distance constraints for weakly oligomerizing sRAGE monomers. Unfortunately, the cysteine chemistry required to introduce PRE paramagnetic groups (Kosen, 1989) prevented the formation of disulfides critical for the structural integrity of the RAGE immunoglobulin domains.

Confocal Microscopy and FRET Assays

Images were acquired using a Zeiss LSM 510 META confocal imaging system equipped with a 30-mW argon laser and an X63, 1.4 NA oil immersion objective. CFP was excited by using a 458 nm laser line at 10% power, and YFP with a 514 nm laser line at 1% power. To minimize channel crosstalk, images were recorded in multi-track mode using a 458/514 beam splitter, with a 467–499 nm emission window for CFP and a 520–595 nm window for YFP. The ImageJ plugin Colocalization Colormap (Jaskolski et al., 2005; Schneider et al., 2012) was used to assess the degree of co-localization of hRAGE with DIAPH1 or DIAPH1ΔDAD. Acceptor photobleaching of selected regions for FRET determination was performed with a 514 nm laser line at 100% power, reducing YFP emission to below 5% of its initial value. Quantitatively, FRET was measured as an increase in CFP fluorescence intensity (donor de-quenching) after YFP (acceptor) photobleaching. Another ImageJ plugin, AccPbFRET version 3.16 (Roszik et al., 2008), was used to process images from the time/bleach series and quantitatively estimate FRET values.

SUPPLEMENTAL INFORMATION

Supplemental Information includes Supplemental Experimental Procedures, seven figures, and two tables and can be found with this article online at <http://dx.doi.org/10.1016/j.str.2016.06.021>.

AUTHOR CONTRIBUTIONS

J.X., M.M., M.S., V.R., and S.R. conducted the experiments, D.F., A.M.S., and A.S. designed the experiments, and J.X., D.S.B., D.F., A.M.S., and A.S. wrote the paper.

ACKNOWLEDGMENTS

This work was supported by NIH grants GM085006 (to A.S.) and 1R24DK103032 (to A.M. S.).

Received: February 8, 2016

Revised: May 20, 2016

Accepted: June 16, 2016

Published: August 11, 2016

REFERENCES

- Angers, S., Salahpour, A., and Bouvier, M. (2002). Dimerization: an emerging concept for G protein-coupled receptor ontogeny and function. *Annu. Rev. Pharmacol. Toxicol.* **42**, 409–435.
- Bernado, P., Garcia de la Torre, J., and Pons, M. (2002). Interpretation of 15N NMR relaxation data of globular proteins using hydrodynamic calculations with HYDRONMR. *J. Biomol. NMR* **23**, 139–150.
- Berry, R., Chen, Z., McCluskey, J., and Rossjohn, J. (2011). Insight into the basis of autonomous immunoreceptor activation. *Trends Immunol.* **32**, 165–170.
- Bianchi, R., Kastrisianaki, E., Giambanco, I., and Donato, R. (2011). S100B protein stimulates microglia migration via RAGE-dependent up-regulation of chemokine expression and release. *J. Biol. Chem.* **286**, 7214–7226.
- Blobel, J., Bernado, P., Xu, H., Jin, C., and Pons, M. (2009). Weak oligomerization of low-molecular-weight protein tyrosine phosphatase is conserved from mammals to bacteria. *FEBS J.* **276**, 4346–4357.
- Camarero, J.A., Shekhtman, A., Campbell, E.A., Chlenov, M., Gruber, T.M., Bryant, D.A., Darst, S.A., Cowburn, D., and Muir, T.W. (2002). Autoregulation of a bacterial sigma factor explored by using segmental isotopic labeling and NMR. *Proc. Natl. Acad. Sci. USA* **99**, 8536–8541.
- Cavanagh, J., Fairbrother, W.J., Palmer, A.G., Rance, M., and Skelton, N.J. (2007). *Protein NMR Spectroscopy: Principles and Practice*, Second Edition (San Diego: Academic Press).
- Choudhuri, K., Wiseman, D., Brown, M.H., Gould, K., and van der Merwe, P.A. (2005). T-cell receptor triggering is critically dependent on the dimensions of its peptide-MHC ligand. *Nature* **436**, 578–582.
- Chu, F., Shan, S.O., Moustakas, D.T., Alber, F., Egea, P.F., Stroud, R.M., Walter, P., and Burlingame, A.L. (2004). Unraveling the interface of signal recognition particle and its receptor by using chemical cross-linking and tandem mass spectrometry. *Proc. Natl. Acad. Sci. USA* **101**, 16454–16459.
- Cowburn, D., Shekhtman, A., Xu, R., Ottesen, J.J., and Muir, T.W. (2004). Segmental isotopic labeling for structural biological applications of NMR. *Methods Mol. Biol.* **278**, 47–56.
- de Vries, S.J., van Dijk, M., and Bonvin, A.M. (2010). The HADDOCK web server for data-driven biomolecular docking. *Nat. Protoc.* **5**, 883–897.
- Dattilo, B.M., Fritz, G., Leclerc, E., Kooi, C.W., Heizmann, C.W., and Chazin, W.J. (2007). The extracellular region of the receptor for advanced glycation end products is composed of two independent structural units. *Biochemistry* **46**, 6957–6970.
- Dawson, P.E., Muir, T.W., Clark-Lewis, I., and Kent, S.B. (1994). Synthesis of proteins by native chemical ligation. *Science* **266**, 776–779.
- DiGabriele, A.D., Lax, I., Chen, D.I., Svahn, C.M., Jaye, M., Schlessinger, J., and Hendrickson, W.A. (1998). Structure of a heparin-linked biologically active dimer of fibroblast growth factor. *Nature* **393**, 812–817.
- Fabris, D., and Yu, E.T. (2010). Elucidating the higher-order structure of biopolymers by structural probing and mass spectrometry: MS3D. *J. Mass Spectrom.* **45**, 841–860.
- Friedhoff, P. (2005). Mapping protein-protein interactions by bioinformatics and cross-linking. *Anal. Bioanal. Chem.* **381**, 78–80.
- Fushman, D. (2012). Determining protein dynamics from (1)5N relaxation data by using DYNAMICS. *Methods Mol. Biol.* **831**, 485–511.
- Garcia de la Torre, J., Huertas, M.L., and Carrasco, B. (2000). HYDRONMR: prediction of NMR relaxation of globular proteins from atomic-level structures and hydrodynamic calculations. *J. Magn. Reson.* **147**, 138–146.
- He, M., Kubo, H., Morimoto, K., Fujino, N., Suzuki, T., Takahashi, T., Yamada, M., Yamaya, M., Maekawa, T., Yamamoto, Y., et al. (2011). Receptor for advanced glycation end products binds to phosphatidylserine and assists in the clearance of apoptotic cells. *EMBO Rep.* **12**, 358–364.
- Heymann, M., Paramelle, D., Subra, G., Forest, E., Martinez, J., Geourjon, C., and Deleage, G. (2008). MSX-3D: a tool to validate 3D protein models using mass spectrometry. *Bioinformatics* **24**, 2782–2783.
- Hofmann, M.A., Drury, S., Fu, C., Qu, W., Taguchi, A., Lu, Y., Avila, C., Kambham, N., Bierhaus, A., Nawroth, P., et al. (1999). RAGE mediates a novel proinflammatory axis: a central cell surface receptor for S100/calgranulin polypeptides. *Cell* **97**, 889–901.
- Hudson, B.I., Kalea, A.Z., Del Mar Arriero, M., Harja, E., Boulanger, E., D'Agati, V., and Schmidt, A.M. (2008). Interaction of the RAGE cytoplasmic domain with diaphanous-1 is required for ligand-stimulated cellular migration through activation of Rac1 and Cdc42. *J. Biol. Chem.* **283**, 34457–34468.
- Jaskolski, F., Mulle, C., and Manzoni, O.J. (2005). An automated method to quantify and visualize colocalized fluorescent signals. *J. Neurosci. Methods* **146**, 42–49.
- Kislinger, T., Fu, C., Huber, B., Qu, W., Taguchi, A., Du Yan, S., Hofmann, M., Yan, S.F., Pischetsrieder, M., Stern, D., et al. (1999). N(epsilon)-(carboxymethyl)lysine adducts of proteins are ligands for receptor for advanced glycation end products that activate cell signaling pathways and modulate gene expression. *J. Biol. Chem.* **274**, 31740–31749.
- Koch, M., Chitayat, S., Dattilo, B.M., Schiefner, A., Diez, J., Chazin, W.J., and Fritz, G. (2010). Structural basis for ligand recognition and activation of RAGE. *Structure* **18**, 1342–1352.
- Kosen, P.A. (1989). Spin labeling of proteins. *Methods Enzymol.* **177**, 86–121.
- Laskowski, R.A.M., MacArthur, M.W., Moss, D.S., and Thornton, J.M. (1993). PROCHECK: a program to check the stereo chemical quality of protein structures. *J. Appl. Crystallogr.* **26**, 283–291.
- Leclerc, E., Fritz, G., Vetter, S.W., and Heizmann, C.W. (2009). Binding of S100 proteins to RAGE: an update. *Biochim. Biophys. Acta* **1793**, 993–1007.
- Liljensiek, B., Weigand, M.A., Bierhaus, A., Nicklas, W., Kasper, M., Hofer, S., Plachky, J., Grone, H.J., Kurschus, F.C., Schmidt, A.M., et al. (2004). Receptor for advanced glycation end products (RAGE) regulates sepsis but not the adaptive immune response. *J. Clin. Invest.* **113**, 1641–1650.
- Liu, D., Xu, R., Dutta, K., and Cowburn, D. (2008). N-terminal cysteinyl proteins can be prepared using thrombin cleavage. *FEBS Lett.* **582**, 1163–1167.
- Maiti, S., Michelot, A., Gould, C., Blanchoin, L., Sokolova, O., and Goode, B.L. (2012). Structure and activity of full-length formin mDia1. *Cytoskeleton (Hoboken)* **69**, 393–405.
- Masse, J.E., and Keller, R. (2005). AutoLink: automated sequential resonance assignment of biopolymers from NMR data by relative-hypothesis-prioritization-based simulated logic. *J. Magn. Reson.* **174**, 133–151.
- Mathys, S., Evans, T.C., Chute, I.C., Wu, H., Chong, S., Benner, J., Liu, X.Q., and Xu, M.Q. (1999). Characterization of a self-splicing mini-intein and its conversion into autocatalytic N- and C-terminal cleavage elements: facile production of protein building blocks for protein ligation. *Gene* **231**, 1–13.
- Medapati, M.R., Dahlmann, M., Ghavami, S., Pathak, K.A., Lucman, L., Klonisch, T., Hoang-Vu, C., Stein, U., and Hombach-Klonisch, S. (2015). RAGE mediates the pro-migratory response of extracellular S100A4 in human thyroid Cancer cells. *Thyroid* **25**, 514–527.
- Meghnani, V., Vetter, S.W., and Leclerc, E. (2014). RAGE overexpression confers a metastatic phenotype to the WM115 human primary melanoma cell line. *Biochim. Biophys. Acta* **1842**, 1017–1027.
- Metzger, H. (1992). Transmembrane signaling: the joy of aggregation. *J. Immunol.* **149**, 1477–1487.
- Neeper, M., Schmidt, A.M., Brett, J., Yan, S.D., Wang, F., Pan, Y.C., Elliston, K., Stern, D., and Shaw, A. (1992). Cloning and expression of a cell surface

- receptor for advanced glycosylation end products of proteins. *J. Biol. Chem.* **267**, 14998–15004.
- Ostendorp, T., Leclerc, E., Galichet, A., Koch, M., Demling, N., Weigle, B., Heizmann, C.W., Kroneck, P.M., and Fritz, G. (2007). Structural and functional insights into RAGE activation by multimeric S100B. *EMBO J.* **26**, 3868–3878.
- Park, H., Adsit, F.G., and Boyington, J.C. (2010). The 1.5 Å crystal structure of human receptor for advanced glycation endproducts (RAGE) ectodomains reveals unique features determining ligand binding. *J. Biol. Chem.* **285**, 40762–40770.
- Rai, V., Maldonado, A.Y., Burz, D.S., Reverdatto, S., Yan, S.F., Schmidt, A.M., and Shekhtman, A. (2012a). Signal transduction in receptor for advanced glycation end products (RAGE): solution structure of C-terminal rage (ctRAGE) and its binding to mDia1. *J. Biol. Chem.* **287**, 5133–5144.
- Rai, V., Toure, F., Chitayat, S., Pei, R., Song, F., Li, Q., Zhang, J., Rosario, R., Ramasamy, R., Chazin, W.J., et al. (2012b). Lysophosphatidic acid targets vascular and oncogenic pathways via RAGE signaling. *J. Exp. Med.* **209**, 2339–2350.
- Ramsland, P.A., Farrugia, W., Bradford, T.M., Sardjono, C.T., Esparon, S., Trist, H.M., Powell, M.S., Tan, P.S., Cendron, A.C., Wines, B.D., et al. (2011). Structural basis for Fc gammaRIIIa recognition of human IgG and formation of inflammatory signaling complexes. *J. Immunol.* **187**, 3208–3217.
- Rao, N.V., Argyle, B., Xu, X., Reynolds, P.R., Walenga, J.M., Prechel, M., Prestwich, G.D., MacArthur, R.B., Walters, B.B., Hoidal, J.R., et al. (2010). Low anticoagulant heparin targets multiple sites of inflammation, suppresses heparin-induced thrombocytopenia, and inhibits interaction of RAGE with its ligands. *Am. J. Physiol. Cell Physiol.* **299**, C97–C110.
- Reverdatto, S., Rai, V., Xue, J., Burz, D.S., Schmidt, A.M., and Shekhtman, A. (2013). Combinatorial library of improved peptide aptamers, CLIPs to inhibit RAGE signal transduction in mammalian cells. *PLoS One* **8**, e65180.
- Rozsik, J., Szollosi, J., and Vereb, G. (2008). AccPbFRET: an ImageJ plugin for semi-automatic, fully corrected analysis of acceptor photobleaching FRET images. *BMC Bioinformatics* **9**, 346.
- Sarkany, Z., Ikonen, T.P., Ferreira-da-Silva, F., Saraiva, M.J., Svergun, D., and Damas, A.M. (2011). Solution structure of the soluble receptor for advanced glycation end products (sRAGE). *J. Biol. Chem.* **286**, 37525–37534.
- Schamel, W.W., and Reth, M. (2000). Monomeric and oligomeric complexes of the B cell antigen receptor. *Immunity* **13**, 5–14.
- Schmidt, A.M., Vianna, M., Gerlach, M., Brett, J., Ryan, J., Kao, J., Esposito, C., Hegarty, H., Hurlley, W., Clauss, M., et al. (1992). Isolation and characterization of two binding proteins for advanced glycosylation end products from bovine lung which are present on the endothelial cell surface. *J. Biol. Chem.* **267**, 14987–14997.
- Schmidt, A.M., Yan, S.D., Yan, S.F., and Stern, D.M. (2001). The multiligand receptor RAGE as a progression factor amplifying immune and inflammatory responses. *J. Clin. Invest.* **108**, 949–955.
- Schneider, C.A., Rasband, W.S., and Eliceiri, K.W. (2012). NIH Image to ImageJ: 25 years of image analysis. *Nat. Methods* **9**, 671–675.
- Shimada, A., Nyitrai, M., Vetter, I.R., Kuhlmann, D., Bugyi, B., Narumiya, S., Geeves, M.A., and Wittinghofer, A. (2004). The core FH2 domain of diaphanous-related formins is an elongated actin binding protein that inhibits polymerization. *Mol. Cell* **13**, 511–522.
- Sitkiewicz, E., Tarnowski, K., Poznanski, J., Kulma, M., and Dadlez, M. (2013). Oligomerization interface of RAGE receptor revealed by MS-monitored hydrogen deuterium exchange. *PLoS One* **8**, e76353.
- Su, P.C., and Berger, B.W. (2012). Identifying key juxtamembrane interactions in cell membranes using AraC-based transcriptional reporter assay (AraTM). *J. Biol. Chem.* **287**, 31515–31526.
- Taguchi, A., Blood, D.C., del Toro, G., Canet, A., Lee, D.C., Qu, W., Tanji, N., Lu, Y., Lalla, E., Fu, C., et al. (2000). Blockade of RAGE-amphoterin signalling suppresses tumour growth and metastases. *Nature* **405**, 354–360.
- Tang, C., Ghirlardo, R., and Clore, G.M. (2008). Visualization of transient ultra-weak protein self-association in solution using paramagnetic relaxation enhancement. *J. Am. Chem. Soc.* **130**, 4048–4056.
- Toure, F., Fritz, G., Li, Q., Rai, V., Daffu, G., Zou, Y.S., Rosario, R., Ramasamy, R., Alberts, A.S., Yan, S.F., et al. (2012). Formin mDia1 mediates vascular remodeling via integration of oxidative and signal transduction pathways. *Circ. Res.* **110**, 1279–1293.
- Trakselis, M.A., Alley, S.C., and Ishmael, F.T. (2005). Identification and mapping of protein-protein interactions by a combination of cross-linking, cleavage, and proteomics. *Bioconjug. Chem.* **16**, 741–750.
- Tzeng, S.R., Pai, M.T., and Kalodimos, C.G. (2012). NMR studies of large protein systems. *Methods Mol. Biol.* **831**, 133–140.
- van Zoelen, M.A., Schmidt, A.M., Florquin, S., Meijers, J.C., de Beer, R., de Vos, A.F., Nawroth, P.P., Bierhaus, A., and van der Poll, T. (2009). Receptor for advanced glycation end products facilitates host defense during *Escherichia coli*-induced abdominal sepsis in mice. *J. Infect. Dis.* **200**, 765–773.
- Wassenaar, T.A., Dijk, M., Loureiro-Ferreira, N., Schot, G., Vries, S.J., Schmitz, C., Zwan, J., Boelens, R., Giachetti, A., Ferella, L., et al. (2012). WeNMR: structural biology on the grid. *J. Grid Comput.* **10**, 743–767.
- Wei, W., Lampe, L., Park, S., Vangara, B.S., Waldo, G.S., Cabantous, S., Subaran, S.S., Yang, D., Lakatta, E.G., and Lin, L. (2012). Disulfide bonds within the C2 domain of RAGE play key roles in its dimerization and biogenesis. *PLoS One* **7**, e50736.
- Xie, J., Burz, D.S., He, W., Bronstein, I.B., Lednev, I., and Shekhtman, A. (2007). Hexameric calgranulin C (S100A12) binds to the receptor for advanced glycation end products (RAGE) using symmetric hydrophobic target-binding patches. *J. Biol. Chem.* **282**, 4218–4231.
- Xie, J., Reverdatto, S., Frolov, A., Hoffmann, R., Burz, D.S., and Shekhtman, A. (2008). Structural basis for pattern recognition by the receptor for advanced glycation end products (RAGE). *J. Biol. Chem.* **283**, 27255–27269.
- Xu, R., Ayers, B., Cowburn, D., and Muir, T.W. (1999). Chemical ligation of folded recombinant proteins: segmental isotopic labeling of domains for NMR studies. *Proc. Natl. Acad. Sci. USA* **96**, 388–393.
- Xu, D., Young, J.H., Krahn, J.M., Song, D., Corbett, K.D., Chazin, W.J., Pedersen, L.C., and Esko, J.D. (2013). Stable RAGE-heparan sulfate complexes are essential for signal transduction. *ACS Chem. Biol.* **8**, 1611–1620.
- Xue, J., Rai, V., Singer, D., Chabierski, S., Xie, J., Reverdatto, S., Burz, D.S., Schmidt, A.M., Hoffmann, R., and Shekhtman, A. (2011). Advanced glycation end product recognition by the receptor for AGEs. *Structure* **19**, 722–732.
- Xue, J., Burz, D.S., and Shekhtman, A. (2012). Segmental labeling to study multidomain proteins. *Adv. Exp. Med. Biol.* **992**, 17–33.
- Yan, S.D., Chen, X., Fu, J., Chen, M., Zhu, H., Roher, A., Slattery, T., Zhao, L., Nagashima, M., Morser, J., et al. (1996). RAGE and amyloid-beta peptide neurotoxicity in Alzheimer's disease. *Nature* **382**, 685–691.
- Yatime, L., and Andersen, G.R. (2013). Structural insights into the oligomerization mode of the human receptor for advanced glycation end-products. *FEBS J.* **280**, 6556–6568.
- Zong, H., Madden, A., Ward, M., Mooney, M.H., Elliott, C.T., and Stitt, A.W. (2010). Homodimerization is essential for the receptor for advanced glycation end products (RAGE)-mediated signal transduction. *J. Biol. Chem.* **285**, 23137–23146.

Structure, Volume 24

Supplemental Information

**Change in the Molecular Dimension
of a RAGE-Ligand Complex Triggers RAGE Signaling**

Jing Xue, Michaele Manigrasso, Matteo Scalabrin, Vivek Rai, Sergey Reverdatto, David S. Burz, Daniele Fabris, Ann Marie Schmidt, and Alexander Shekhtman

Supplemental Information

Change in the Molecular Dimension of a RAGE-ligand complex triggers RAGE signaling

Jing Xue¹, Michaele Manigrasso², Matteo Scalabrin¹, Vivek Rai³, Sergey Reverdatto¹, David S. Burz¹, Daniele Fabris¹, Ann Marie Schmidt², Alexander Shekhtman¹

¹ Department of Chemistry, State University of New York at Albany, Albany, NY 12222, USA

² New York University, Langone Medical Center, New York, NY 10016, USA

³ Institute of Life Sciences, Bhubaneswar, Odisha 751023, India

Supplemental Experimental Procedures

Figure S1. Identification of CL-sRAGE.

Figure S2. Changes in chemical shifts and intensities of VC1 and C2 domain peaks due to chemical ligation and dimerization.

Figure S3. CL-sRAGE is an oligomer

Figure S4. The model homo-dimer structure of sRAGE is consistent with CL-sRAGE NMR relaxation data.

Figure S5. Changes in the chemical shifts and intensities of the VC1 domain in CL-RAGE and Ca²⁺- S100B peaks due to the binding interaction.

Figure S6. MS analysis of the Ca²⁺- S100B-CL-sRAGE- complex.

Figure S7. Active DIAPH1, ΔDAD-DIAPH1, interacts with RAGE in the absence of RAGE ligands.

Table S1. AIRs and unambiguous distance constraints used in the docking experiments.

Table S2. Statistics of the docked complexes.

Supplemental Experimental Procedures.

Reagents and Chemicals

Sodium 2-mercaptoethanesulfonate (MESNA) was from Sigma-Aldrich Co. Restriction enzymes and *Taq* polymerase were from NEB. Cross-linking reagents bis-sulfosuccinimidyl suberate (BS3), Sulfo-SMCC and SM(PEG)₆ NHS-PEG-Maleimide Crosslinkers, Trypsin and Glu-C were from Thermo Scientific. All other chemicals used were reagent grade or better.

Cloning, Expression and Purification of free VC1 domain

DNA coding for VC1 fragments (amino acids 23-243) were PCR amplified using oligonucleotides 5'-TTTCATATGGCTCAAAACATCACAGCCCGGATTGG and 5'-GACCTCCTCCAGGTAAACCACCACCTCGAGTTT-3' containing 5'-*Nde*I and 3'-*Xho*I restriction sites. DNA fragments were subcloned into the *Nde*I and *Xho*I sites of pET15b (Novagen), which confers ampicillin resistance. The resulting plasmid, pET15b-VC1, expresses an N terminal His-tagged VC1 domain.

E. coli strain Origami B(DE3) (Novagen) was transformed with pET15b-VC1, grown at 37 °C to an OD₆₀₀ of ~0.8, re-equilibrated to 20 °C for 30 min, induced with 1 mM IPTG, and allowed to express for 4-6 hours. Cells were lysed at 4 °C in lysis buffer (20 mM Tris-HCl [pH 8.0], 20 mM imidazole, 300 mM NaCl) in the presence of lysozyme (5 mg/mL), followed by sonication (5 min with a 50% duty cycle). Clarified lysate was initially purified on a Ni-NTA (Qiagen) column equilibrated with lysis buffer and eluted with 20 mM Tris-HCl [pH 8.0], 250 mM imidazole, 300 mM NaCl. The His-tag was cleaved by thrombin (Novagen) at room temperature for 1 h before gel filtration chromatography on a SE-75 column (Amersham Biosciences). Fractions containing the eluted protein were concentrated by using Amicon-Ultra-Centricones (Millipore). Residual endotoxin was removed from the sample by repetitive use of EndoTrap Red (Lonza). The endotoxin level of the final protein solution was determined by Gel Clot LAL Assay (Lonza) to be less than 0.1 EU/mL. Purity was estimated to be >95% by Coomassie-stained SDS-PAGE.

Cloning, Expression and Purification of N-terminal Thiol-containing C2 domain

Oligonucleotides 5'-GTTGACGTCCGAGACACCCTACTCAGCTGTTT-3' and 5'-TTTTTCCATGGGCAGCAGCCATCATCATCATCATCACAGCAGCGGCCTGGTGC CGCGCTGCAGC-3', which contain 5'-*NcoI* and 3'-*SalI* restriction sites, were used to clone an N-terminal His-tag and thrombin cleavage site, LVPRC, into pET28-C2²⁹ to yield pCL-sRAGE C2. pCL-sRAGE C2 expresses the C2 domain which, when cleaved with thrombin, yields an N-terminal thiol group suitable for chemical ligation (**Figure 1a**).

E. coli strain BL21(DE3) Codon+ (Novagen) was transformed with pET28-CL-sRAGE C2, and grown in LB medium at 37 °C for 16 hours. The cells were transferred into a secondary medium, induced with 1 mM isopropyl β-D-thiogalactoside (IPTG) for another 16 hours at 37 °C, harvested and stored at -80 °C. For [*U*-¹⁵N] labeled proteins, the secondary medium was replaced with M9 minimal medium, supplemented with 0.1% (w/v) [¹⁵N]-NH₄Cl. Frozen cells were re-suspended in 20 mM HEPES, pH 7.0, containing 8 M urea and heat shocked at 100 °C for 10 min. The resulting lysate was clarified by centrifugation and the supernatant was loaded onto a Ni-NTA column. The column was washed with 20 mM HEPES, pH 7.0, 8 M urea. The protein was re-natured on the column by washing with 5 column volumes of 20 mM HEPES buffer, pH 7.0, and the protein was eluted with 20 mM HEPES, pH 7.0, 250 mM imidazole. Fractions containing the eluted protein were pooled and dialyzed into chemical ligation buffer, 20 mM potassium phosphate, pH 7.2, 500 mM NaCl.

Cloning, Expression and Purification of VC1 domain containing C-terminal Thioester-

DNAs coding for the VC1 domain was PCR amplified from pET15b-VC1¹⁵ using oligonucleotides 5'-TTTCATATGGCTCAAACATCACAGCCCGGATTGG-3' and 5'-GGGGCACAGACCCTCGGACCCACGTAGTGCCCTCTACGTGATCATT-3' containing 5'-*NdeI* and 3'-*SpeI* restriction sites. The resulting PCR products were cloned into pTXB1 to yield pTXB1-VC1. pTXB1 encodes the GyrA intein with a single mutation, N198A, which prevents cleavage of the intein-C-extein peptide bond. pTXB1-VC1 was used as a template to introduce a K52A mutation into the VC1 domain by using the QuikChange site-directed mutagenesis kit (Stratagene). pTXB1-VC1-K52A, expresses a K52A mutant VC1 domain-GyrA intein-chitin binding domain (CBD) C-terminal fusion (**Figure 1A**).

E. coli Origami B(DE3) cells were transformed with pTXB1--VC1-K52A , grown in LB medium at 37 °C overnight to an OD₆₀₀ of ~0.8, re-equilibrated to 20 °C for 30 min, induced with 1 mM IPTG, and allowed to express for 5 hours.. For [*U*-¹³C, ¹⁵N] labeling, cells were grown and induced in M9 minimal medium, supplemented with 0.1% (w/v) [¹⁵N]-NH₄Cl and 0.2% (w/v) [¹³C]-glucose. Following over-expression cells were harvested and pressure lysed by using a French pressure cell. Fusion proteins were loaded onto an affinity chromatography column of chitin resin (NEBioLabs), washed with 20 mM sodium phosphate buffer, pH 7.2, 500 mM NaCl, and cleaved on the column in 20 mM sodium phosphate buffer, pH 7.2, 500 mM NaCl, containing 40 mM sodium 2-sulfanylethanesulfonate, MESNA, at 30 °C for 20 h, eluted, and dialyzed into chemical ligation buffer, 20 mM sodium phosphate, pH 7.2, 500 mM NaCl.

Expression and Purification of S100B

One liter of *E. coli* strain N99/pSS2 was grown in LB medium supplemented with 40 mg/L of carbenicillin in a 2.8 L Fernbach flask at 37 °C with vigorous shaking to an OD₆₀₀ of 0.7. 1 mM IPTG was added, and growth was continued for 3-4 h. The cells were harvested by centrifugation, washed once with 50 mM Tris-HCl, pH 8.0, 5 mM MgCl₂, and stored at -80 °C. All fractionation steps were performed at 4 °C. Cells were re-suspended in a volume of 50 mM Tris-HCl, pH 8.0, 5 mM MgCl₂ equal to 10 times their packed weight, and disrupted by one passage through a French pressure cell at 20,000 psi. Cell debris was removed by centrifugation for 15 min at 12,000 rcf. The supernatant solution was centrifuged for 90 min at 150,000 rcf. Ammonium sulfate was added to the supernatant to 90% of saturation to precipitate unwanted protein. After the supernatant was collected, the pH was adjusted to 4 by adding 10% (v/v) formic acid and stirred at 4 °C for an additional 30 min. The precipitate was collected by centrifugation at 12,000 rcf for 15 min, re-dissolved in 25 mM Tris-HCl, pH 8.0, 1 mM EDTA, 1 mM DTT, and dialyzed overnight against the same buffer.

The dialyzed sample was applied to a HiTrap™ Q FF column (GE Healthcare). The column was equilibrated at 1 mL/min in 100% buffer A, 25 mM Tris-HCl, pH 8.0, 1 mM EDTA, 1mM DTT, and elution was monitored at 280 nm. The protein was eluted using a gradient of 0-1 M NaCl over 30 minutes. S100B eluted at 0.43 M NaCl and appeared as a single band on SDS-PAGE. The purity of the protein was confirmed by electrospray mass spectrometry analysis.

In-gel Digestion

Cross-linked CL-sRAGE bands were cut from Coomassie-stained SDS polyacrylamide gels and divided into pieces $\sim 1 \text{ mm}^3$ in volume. The pieces were destained for 3 h in 0.5 mL of 50% methanol and 5% acetic acid. The solution was refreshed once after 2 hours. After destaining, three 200 μL aliquots of acetonitrile were used to dehydrate the gel fragments. Acetonitrile was discarded and the fragments were dried. The fragments were reduced by adding 30 μL of 10 mM DTT, and chemically modified by adding 30 μL of 50 mM iodoacetamide at room temperature for 30 min, followed by a 100 μL wash of 100 mM ammonium bicarbonate for 10 min and dehydration with 200 μL of acetonitrile for 5 min. After rehydration with 200 μL of 100 mM ammonium bicarbonate and dehydrating two more times, the gel fragments were dried in a speed vacuum for 2-3 min. Digestion was accomplished by adding 50 μL of 20 ng/ μL endoproteinase Trypsin and 100 ng/ μL of endoproteinase GluC (*Staphylococcus aureus* Protease V8) and incubating on ice for 30 min. Excess enzyme solution was removed and an additional 20 μL aliquot of 50 mM ammonium bicarbonate was added and incubated overnight at 37 °C. The digested peptides were extracted by using 10 μL of 5% formic acid followed by 20 μL of 5% formic acid and 50% acetonitrile. The peptide solution was lyophilized, and re-dissolved in 50 μL of 1% acetic acid.

Enzyme-Linked Immunosorbent Assay (ELISA)

To estimate the binding affinity of CL-sRAGE for S100B, we used purified CL-sRAGE and Bovine brain S100B protein (Calbiochem). 96-well plates (Falcon ProBind, Becton Dickinson) were coated with CL-sRAGE at 20 ng/well in 0.1 M sodium carbonate buffer, pH 9.6, overnight at 4 °C. Wells were blocked with wash buffer (20 mM Tris-HCl, pH 7.0, 100 mM Na_2SO_4 , 1 mM CaCl_2) containing 1% BSA (Fraction V, Calbiochem), and incubated at room temperature for 2 hours. S100B, in wash buffer, at concentrations ranging from 0-10 μM , was added to the wells and the samples incubated for 2 h at room temperature. Mouse monoclonal [6G1] anti-S100B HRP conjugate antibody (Abcam) diluted 1:1000-1:3000 in wash buffer containing 1% BSA was added to each well and incubated for 3 h at room temperature or overnight at 4 °C. After adding chromogenic TMB substrate solution (Thermo Scientific), plates were read on a scanner. All washes between steps were performed 4-6 times using wash buffer. Data was analyzed by using GraphPad Prism 5 software.

Sample preparation for NMR Spectroscopy.

Protein samples of free [U - ^{15}N]-C2, free [U - ^2D , ^{15}N]-VC1 and CL-sRAGE constructs, [U - ^{15}N , ^2H]-VC1-C2 and VC1-[U - ^{15}N]-C2, were dissolved in NMR buffer (20 mM sodium phosphate pH 7.0, 100 mM Na_2SO_4 , 0.5 mM DTT, 1 mM EDTA, 90%/10% $\text{H}_2\text{O}/\text{D}_2\text{O}$) at concentrations ranging from 40 μM to 100 μM . To create the CL-sRAGE- Ca^{2+} -S100B complex, 0.5 mM of either unlabeled or [U - ^{15}N]-S100B was added to samples of either 60 mM VC1-[U - ^{15}N]-C2 or 80 mM [U - ^{15}N , ^2H]-VC1-C2, dissolved in 20 mM Tris-HCl (D_{11} , 98% enrichment) pH 7.0, 100 mM Na_2SO_4 , 0.5 mM DTT, 1 mM Ca_2Cl , 90%/10% $\text{H}_2\text{O}/\text{D}_2\text{O}$. DTT was added to 0.5 mM to maintain the reduced state of the cysteines introduced into the CL-sRAGE linker during chemical ligation. Previously, we observed that reducing disulfide bonds within either VC1 or C2 domains results in sRAGE unfolding (Xie et al., 2007; Xie et al., 2008; Xue et al., 2011). Since the NMR spectra of CL-sRAGEs indicate that the protein is folded, we concluded that the CL-sRAGE constructs contain intact disulfide bonds.

Hydrodynamic Calculations

^{15}N -NMR relaxation rates for monomers and dimers were calculated by using the program HydroNMR (Garcia de la Torre et al., 2000). The atomic radius was assigned to be 2 Å and the (N-H) atomic distance 1.02 Å. The temperature was set to 25 °C, the viscosity to $8.1 \cdot 10^{-3}$ poise and the NMR field strength to 16.45 T. For CL-sRAGE monomers, a rotational correlation time of $\tau_{\text{cM}} = 16.5$ ns ($\langle R_2/R_1 \rangle = 40$) was calculated, with an anisotropy of $D_{\text{par}}/D_{\text{per}} = 1.3$. The dimer had a τ_{cD} value of 32.33 ns ($\langle R_2/R_1 \rangle = 135$) and $D_{\text{par}}/D_{\text{per}} = 0.83$, consistent with it being the most anisotropic species.

^{15}N -NMR Relaxation Data Analysis

^{15}N -NMR relaxation data were filtered for fitting as described elsewhere (Blobel et al., 2009; Blobel et al., 2007; Fushman, 2012). Briefly, data from individual residues were not used when any of the following three situations were encountered: (a) Heteronuclear Overhauser Effect < 0.6 , (b) large ($> 25\%$) experimental errors when compared with the relaxation rates R_2/R_1 , where R_1 and R_2 correspond to longitudinal and transverse relaxation, respectively, and (c) large disagreement ($> 25\%$) between the experimental and simulated R_2/R_1 values using the relevant model, filtering for residues affected by chemical exchange. A total of 71 experimental R_2/R_1

values were extracted from CL-sRAGE at two concentrations, 40 μM and 80 μM . The average relative relaxation rates ($\langle R_2/R_1 \rangle$) were calculated for each protein concentration.

Experimental R_1 and R_2 values represent the concentration weighted average of the relaxation rates of all participating species. Equation (1) shows the calculation of the relaxation rates for the monomer–dimer model, where M is the molar fraction of monomer, D is the molar fraction of dimer, P is the population of monomer, P_M , or dimer, P_D .

$$R_n = p_M R_{n,M} + p_D R_{n,D} \quad , \quad (1)$$

The relaxation rate R_n of each species is denoted with the subscript n , which is equal to 1 and 2 in the case of longitudinal and transverse relaxation, respectively. The equilibrium parameters were determined by minimizing the error function:

$$X^2 = \frac{1}{N} \times \left(\sum_i \sum_j \left[\left(\frac{R_2}{R_1} \right)_{ij}^{exp} - \left(\frac{R_2}{R_1} \right)_{ij}^{theo} \right]^2 \div \left[E \left(\frac{R_2}{R_1} \right)_{ij}^{exp} \right]^2 \right) \quad , \quad (2)$$

where i and j denote different residues (i) at varying protein concentrations (j), $E(R_2/R_1)^{exp}$ is the corresponding experimental error, and N is the number of experimental data sets.

Fitting theoretical relaxation rates of two species to experimental values using a monomer-dimer model requires that only the dissociation constant, K_d , be adjusted.

$$K_d = \frac{[M]^2}{[D]} = \frac{2P_M^2}{P_D} c \quad , \quad (3)$$

where c is the total protein concentration and ($P_M + P_D = 1$). The minimization protocol consists of a grid search for each variable using the function “fmincon” as implemented in Matlab (MathWork Inc).

hRAGE and DIAPH1 Fusions with Fluorescent Proteins

Construction of human RAGE-mYFP was described previously (Xie et al., 2008). A fragment containing human *Diaphanous-1* cDNA was PCR amplified using source clone #401258087 (Open Biosystems) as a template, and inserted into a modified Clontech vector pmCFP-N1(Xie et al., 2008) at *XhoI* and *AgeI* sites, upstream of a fluorescent protein sequence, to obtain DIAPH1-mCFP. Deletion of the 3'-terminus of *DIAPH1* containing the *DAD domain* (aa 1194-1272) was performed using the QuikChange site-directed mutagenesis II-E kit (Stratagene) resulting in construct DIAPH1 Δ DAD-mCFP.

Sample preparation for confocal microscopy.

HEK293 cells were plated on 15 mm glass coverslips from Ted Pella, Inc (Redding, CA) and treated with collagen type IV from human placenta (Sigma). Cells were grown at 37 °C, with 5% CO₂ in low glucose DMEM medium (Thermo Scientific) supplemented with 10% FBS, to 50-70% confluency. DIAPH1-mCFP, DIAPH1ΔDAD-mCFP (donor) or hRAGE-mYFP (acceptor) plasmids were introduced into the cells separately or simultaneously with the help of TransIT-293 transfection reagent (MirusBio LLC, Madison, WI). Prior to transfection the medium was exchanged with Opti-MEM (Invitrogen) supplemented with 5% FBS. Cells were incubated with transfection mix for 16 hours, the medium was then replaced with Opti-MEM/0.1% FBS and incubated for additional 6 hours. Appropriate wells were treated with RAGE ligand S100B (EMD Millipore) at a final concentration of 0.5 μM for 0, 10 or 60 minutes. Cells were fixed by adding equal volume of 4% formaldehyde in 1X PBS for 20-30 minutes at 37 °C, washed 3X with 1 mL of 1X PBS and mounted on slides with Fluoromount G (Electron Microscopy Sciences, Hatfield, PA).

Cell Lines.

Wild-type (WT) and DIAPH1 knockout (DIAPH1 KO) primary murine aortic vascular smooth muscle cells (SMC) were isolated and employed through passages 5 to 7. Vascular SMCs were grown in 10% FBS containing DMEM medium (Invitrogen)(Toure et al., 2012).

Stimulation assay.

SMCs were seeded at 1×10^6 cells/100 mm dish in complete medium and grown for 24 h before subjecting them to overnight starvation in serum-free medium. The next day cells were stimulated with 10 μg/mL of S100B-BSA for five minutes at 37 °C. Cells were rinsed with ice-cold PBS and lysed using lysis buffer (Cell Signaling Technology) containing 1 mM phenylmethylsulfonyl fluoride and Complete Protease Inhibitors (Roche Applied Science).

Western Blotting.

Total SMC lysates were immunoblotted and probed with AKT-specific antibody, and phospho-AKT-specific antibody. Antibody to DIAPH1 was obtained from Santa Cruz Biotechnology. After probing with the primary antibodies, membranes were stripped and reprobed for relative total AKT protein. Donkey anti-rabbit HRP-conjugated-IgG (Amersham Pharmacia Biotechnology) or sheep anti-mouse HRP-conjugated-IgG (Amersham Pharmacia

Biotechnology) was used to identify sites of binding of the primary antibody where indicated. Blots were scanned by using an AlfaImager TM 2200 scanner with AlfaEase (AlfaImager) FC 2200 software. Results are reported as the relative absorbance of test antigen to relative total protein. In all Western blot studies, at least triplicate cell lysates per group were used; results of representative experiments are shown.

Supplemental References.

Blobel, J., Bernado, P., Xu, H., Jin, C., and Pons, M. (2009). Weak oligomerization of low-molecular-weight protein tyrosine phosphatase is conserved from mammals to bacteria. *The FEBS journal* *276*, 4346-4357.

Blobel, J., Schmidl, S., Vidal, D., Nisius, L., Bernado, P., Millet, O., Brunner, E., and Pons, M. (2007). Protein tyrosine phosphatase oligomerization studied by a combination of ¹⁵N NMR relaxation and ¹²⁹Xe NMR. Effect of buffer containing arginine and glutamic acid. *Journal of the American Chemical Society* *129*, 5946-5953.

Fushman, D. (2012). Determining protein dynamics from (1)(5)N relaxation data by using DYNAMICS. *Methods in molecular biology* *831*, 485-511.

Garcia de la Torre, J., Huertas, M.L., and Carrasco, B. (2000). HYDRONMR: prediction of NMR relaxation of globular proteins from atomic-level structures and hydrodynamic calculations. *J Magn Reson* *147*, 138-146.

Toure, F., Fritz, G., Li, Q., Rai, V., Daffu, G., Zou, Y.S., Rosario, R., Ramasamy, R., Alberts, A.S., Yan, S.F., *et al.* (2012). Formin mDia1 mediates vascular remodeling via integration of oxidative and signal transduction pathways. *Circ Res* *110*, 1279-1293.

Xie, J., Burz, D.S., He, W., Bronstein, I.B., Lednev, I., and Shekhtman, A. (2007). Hexameric calgranulin C (S100A12) binds to the receptor for advanced glycated end products (RAGE) using symmetric hydrophobic target-binding patches. *The Journal of biological chemistry* *282*, 4218-4231.

Xie, J., Reverdatto, S., Frolov, A., Hoffmann, R., Burz, D.S., and Shekhtman, A. (2008). Structural basis for pattern recognition by the receptor for advanced glycation end products (RAGE). *The Journal of biological chemistry* *283*, 27255-27269.

Xue, J., Rai, V., Singer, D., Chabierski, S., Xie, J., Reverdatto, S., Burz, D.S., Schmidt, A.M., Hoffmann, R., and Shekhtman, A. (2011). Advanced glycation end product recognition by the receptor for AGEs. *Structure* 19, 722-732.

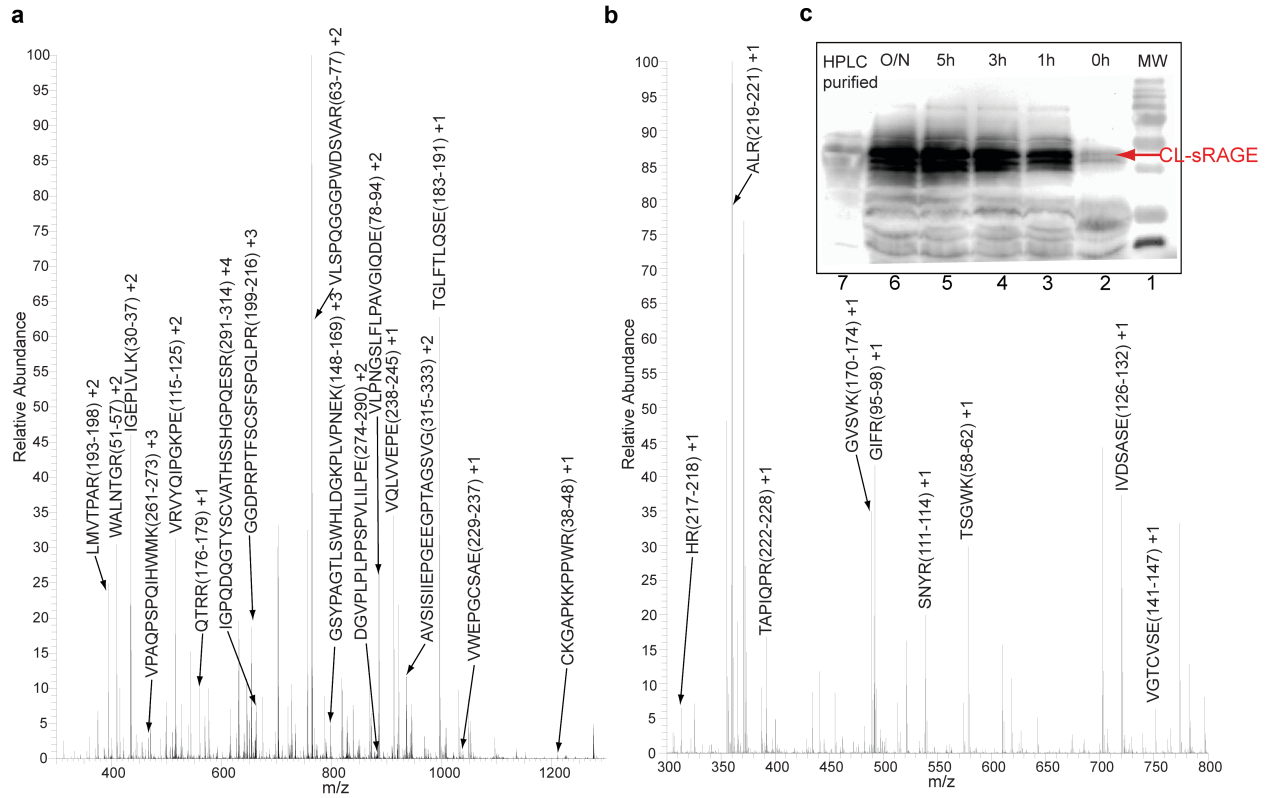


Figure S1. Related to Figure 1. Identification of CL-sRAGE. (a,b) CL-sRAGE was digested with Trypsin and Glu-C at room temperature for 16 hours. Peptide coverage reached 90% by mass spectrometry analysis. Peptides in *A* and *B* were separately isolated from a C-18 column using 70% and 0% acetonitrile, respectively. (c) Western analysis of the chemical ligation reaction time-course. From right to left, lane 1 is molecular weight markers; lanes 2, 3, 4, 5 and 6 are time points taken at 0 h, 1 h, 3 h, 5 h and overnight; lane 7 is CL-sRAGE purified by using HPLC chromatography. CL-sRAGE is indicated by the red arrow.

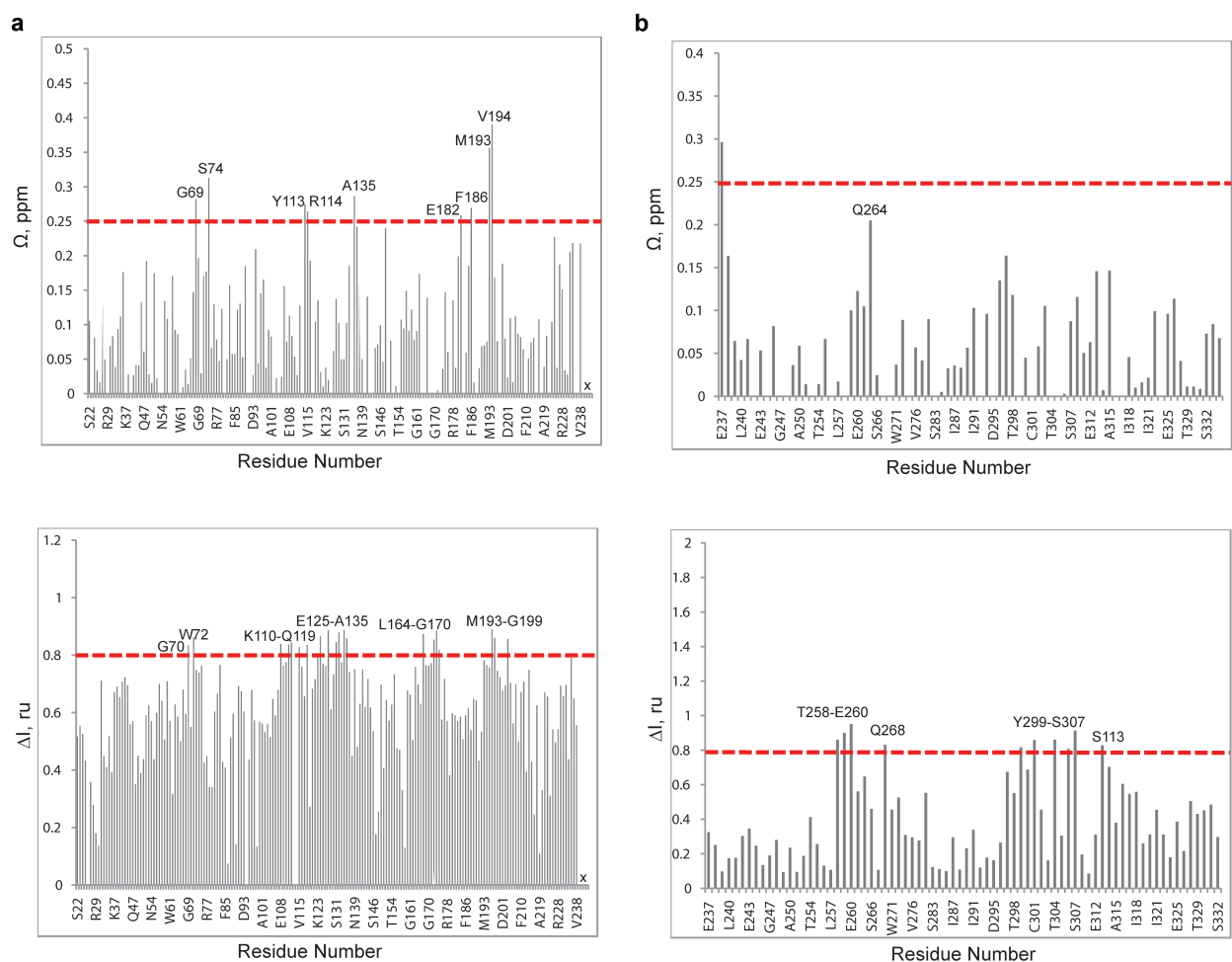


Figure S2. Related to Figure 2. Changes in chemical shifts and intensities of VC1 and C2 domain peaks due to chemical ligation and dimerization. (a) Changes in the $^1\text{H}, ^{15}\text{N}$ -HSQC NMR chemical shifts (top) and signal intensities (bottom) of $[U-^2\text{H}, ^{15}\text{N}]$ -VC1 upon ligation with the C2 domain. (b) Changes in the $^1\text{H}, ^{15}\text{N}$ -HSQC NMR chemical shifts (top) and signal intensities (bottom) of $[U-^{15}\text{N}]$ -C2 upon ligation with the VC1 domain.

Chemical shift changes (Ω) were calculated by $\Omega = \sqrt{\Delta\delta_H^2 + \left(\frac{\Delta\delta_N}{4}\right)^2}$, where $\Delta\delta_H$ and $\Delta\delta_N$ are the changes in amide proton and nitrogen chemical shifts, respectively. Residues that exhibited chemical shift changes above 0.25 ppm were considered to constitute the interaction surfaces. Cut-offs for selecting residues involved in the interaction are indicated by red dashed lines.

NMR signal intensity changes were calculated by using $\Delta I = (I_f - I_l)/I_f$, where $I_{f(l)}$ is the NMR signal intensity. Most of the VC1 residues exhibited uniform broadening upon complex formation. Residues that exhibited signal broadening above 80% were considered to constitute the VC1 interaction surface.

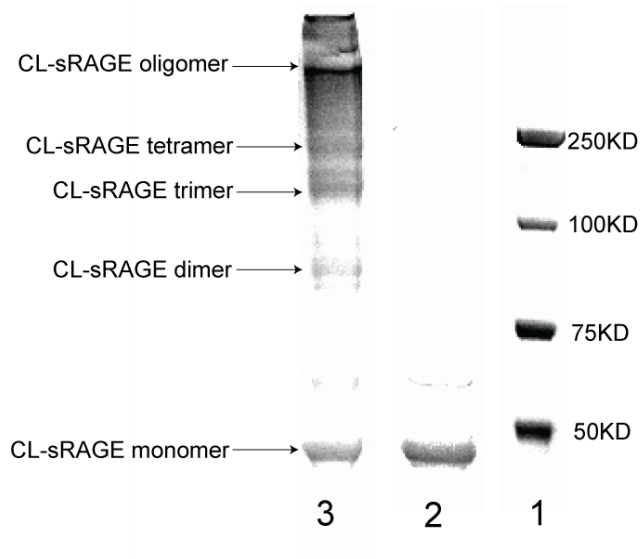


Figure S3. Related to Figure 3. CL-sRAGE is an oligomer. SDS-PAGE of CL-sRAGE crosslinking using BS_3 . Lane 1 is molecular weight markers; lane 2 is purified CL-sRAGE monomer; lane 3 is crosslinked CL-sRAGE. Labeled CL-sRAGE dimers, trimers, and tetramers are located at ~90 kDa, 125 kDa and 200 kDa. At the very top an oligomer greater than 250 kDa is evident.

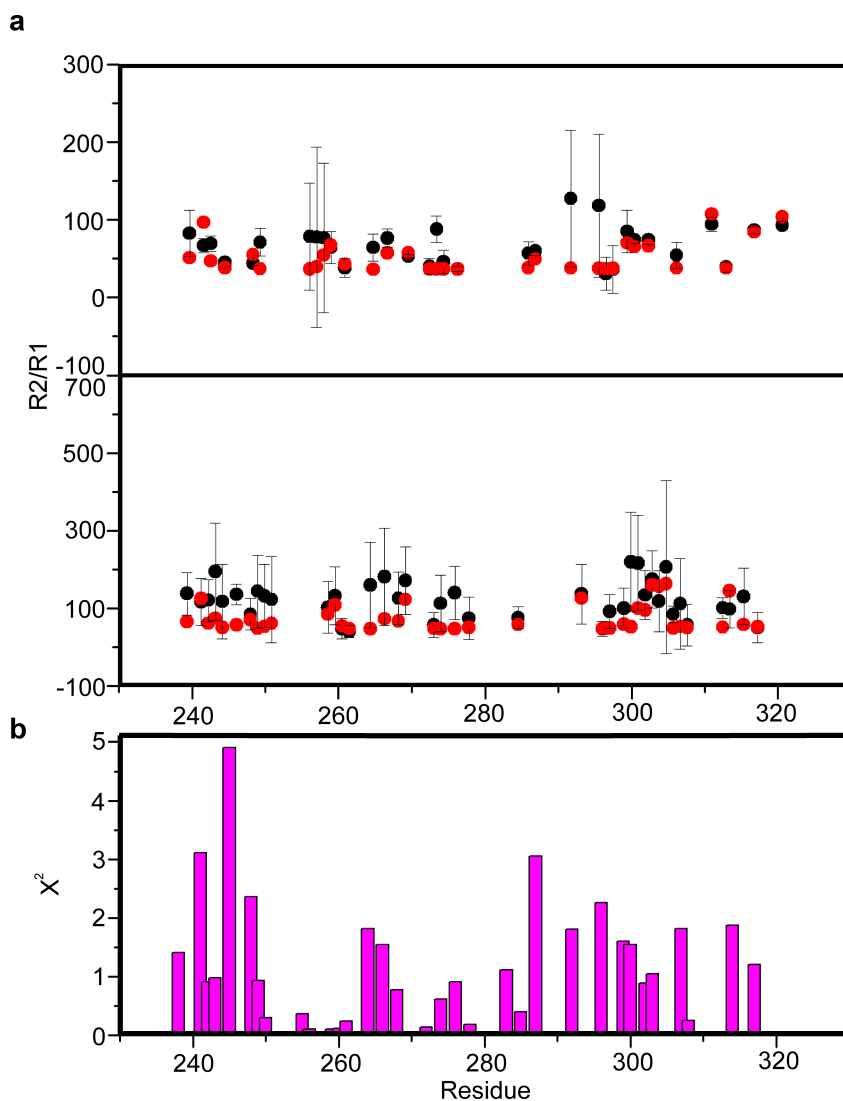


Figure S4. Related to Figure 4. The model homo-dimer structure of sRAGE is consistent with CL-sRAGE NMR relaxation data. (a) R_2/R_1 values of individual residues on the C2 domain in CL-sRAGE (black) were measured at two concentrations: 20 μM (upper panel) and 80 μM (lower panel). Values calculated using the best-fit parameters for a monomer–dimer model are shown in red. **(b)** The average contribution of both experiments to the fitting error of individual residues for the monomer–dimer model.

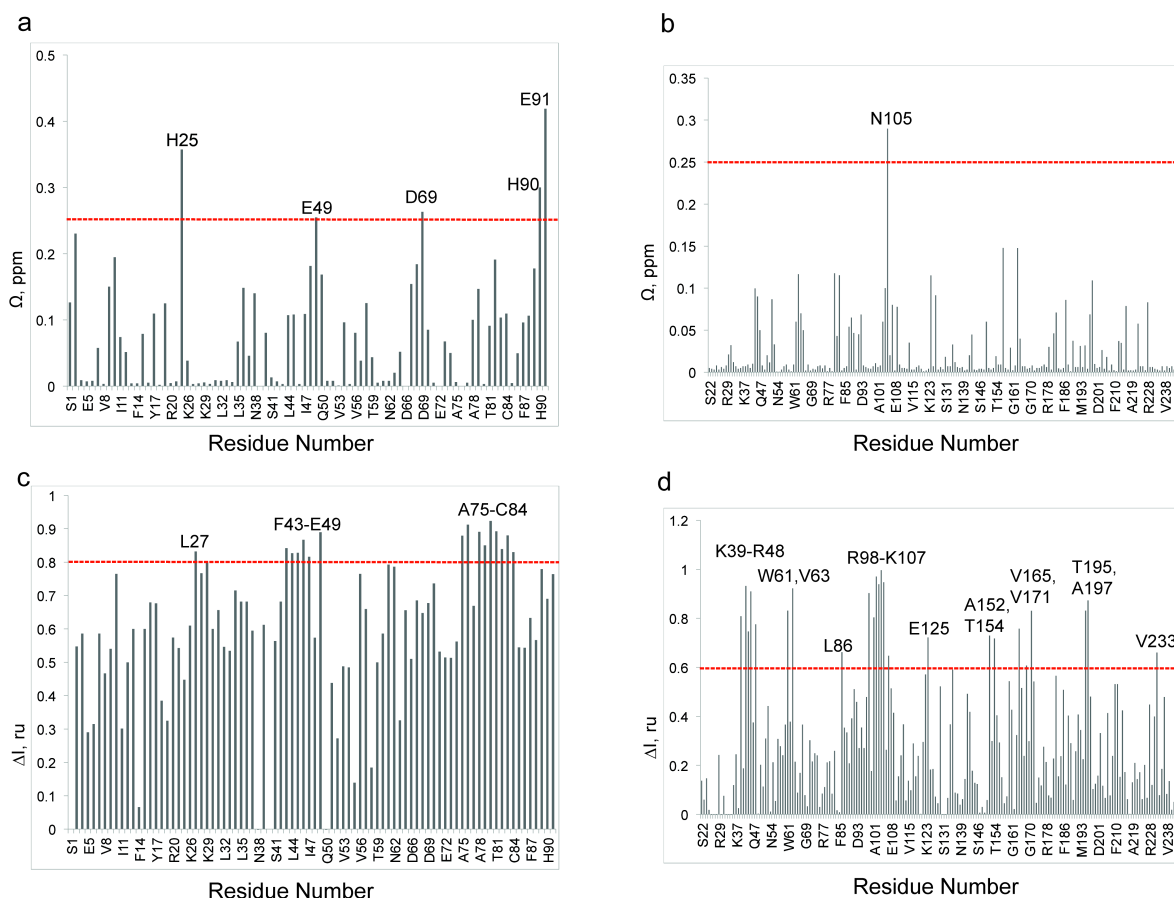


Figure S5. Related to Figure 5. Changes in the chemical shifts and intensities of the VC1 domain in CL-RAGE and S100B peaks due to the binding interaction. (a) Changes in the ^1H , ^{15}N -HSQC NMR chemical shifts (top) and signal intensities (bottom) of $[U\text{-}^{15}\text{N}]\text{-Ca}^{2+}\text{-S100B}$ due to interaction with the VC1 domain. (b) Changes in the ^1H , ^{15}N -HSQC NMR chemical shifts (top) and signal intensities (bottom) of $[U\text{-}^2\text{H}, ^{15}\text{N}]\text{-VC1}$ due to interaction with S100B.

Chemical shift changes (Ω) were calculated by $\Omega = \sqrt{\Delta\delta_H^2 + \left(\frac{\Delta\delta_N}{4}\right)^2}$, where $\Delta\delta_H$ and $\Delta\delta_N$ are the changes in amide proton and nitrogen chemical shifts, respectively. Residues that exhibited chemical shift changes above 0.25 ppm, were considered to constitute the CL-sRAGE- Ca^{2+} -S100B interaction surfaces. Cut-offs for selecting residues involved in the interaction are indicated by red dashed lines.

NMR signal intensity changes were calculated by $\Delta I = (I_f - I_i)/I_f$, where $I_{(f)}$ is the NMR signal intensity. Most of the VC1 and Ca^{2+} -S100B residues exhibited uniform broadening upon

complex formation. Residues that exhibited signal broadening above 80% were considered to constitute the CL-sRAGE-Ca²⁺-S100B interaction surface.

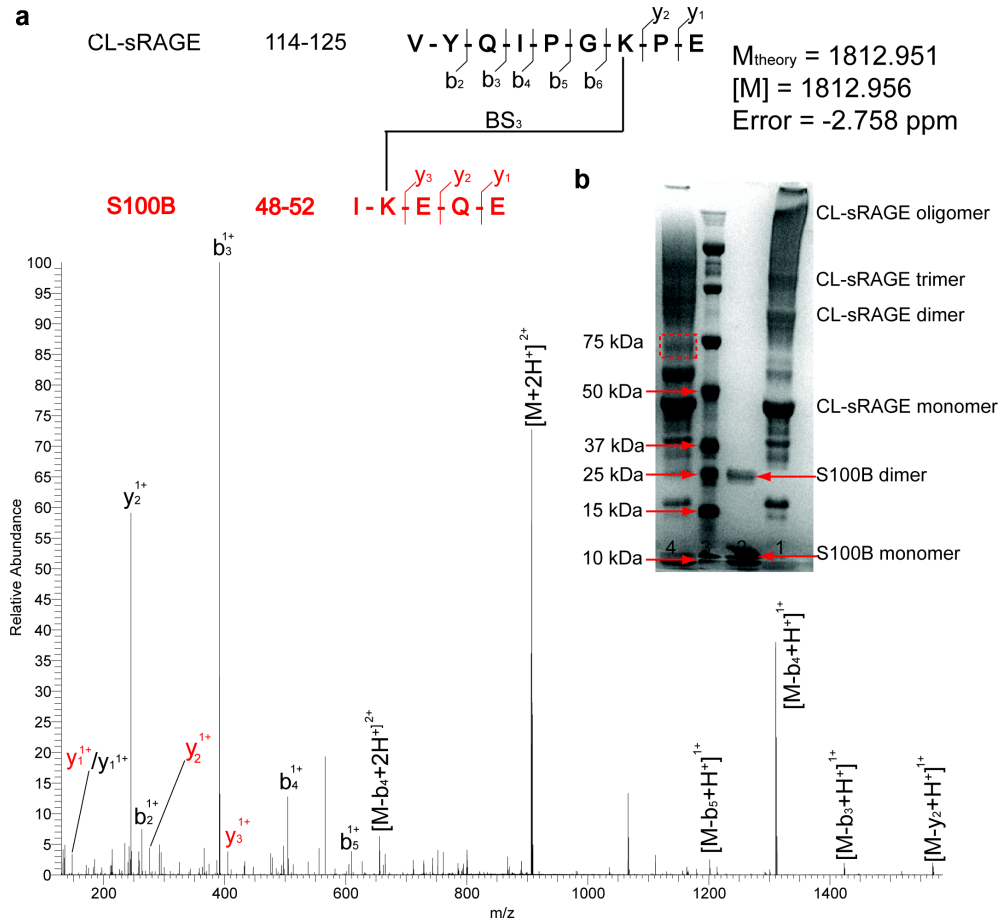


Figure S6. Related to Figure 5. MS analysis of the Ca^{2+} -S100B-CL-sRAGE-complex (a) Peptide composition and residue detected ion fragments of the cross-linked peptide. The HCD spectrum of the cross-linked product, at m/z value of 905.487^{2+} , is consistent with the theoretical monoisotopic mass of 1812.951. Observed fragment ions and their charge states are labeled according to standard nomenclature. Black and red colors, respectively, represent each peptide in the cross-linked product. Coverage of almost all ion fragments (y and b fragment ions) and the involvement of BS₃ in many peptide pieces supports the identity of this cross-linked product, and providing an upper distance constraint between the cross-linked residues equal to the BS₃ spacer arm length of 11.4 Å. **(b)** Gradient (4% - 12%) SDS-PAGE gel of CL-sRAGE BS₃ crosslinks with S100B. Lane 1 is CL-sRAGE self-crosslinks; lane 2 is S100B self-crosslinks with BS₃, displaying both monomers and dimers; lane 3 is the molecular marker; lane 4 is CL-sRAGE crosslinks with S100B, and the red circle indicates a new band distinguishable from CL-sRAGE and S100B self-crosslinking.

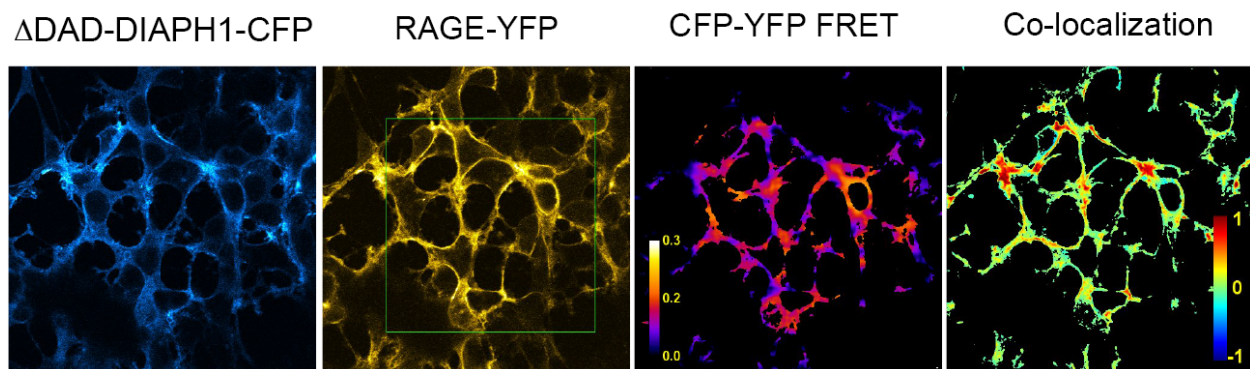


Figure S7. Related to Figure 6. Active DIAPH1, Δ DAD-DIAPH1, interacts with RAGE in the absence of RAGE ligands. Constitutively active Δ DAD-DIAPH1-CFP, in which DAD is removed, readily co-localizes with RAGE, $nMDF=0.091 \pm 0.001$. $nMDF=-1$ signifies no co-localization and $nMDF=1$ is 100% co-localization between CFP and YFP. Forster resonance transfer, FRET, experiments were used to assess the strength of the molecular interaction between fluorescently labeled RAGE-YFP and Δ DAD-DIAPH1-CFP. The increase in donor, RAGE-CFP, emission due to acceptor, Δ DAD-DIAPH1-CFP, photobleaching in the region shown by the green rectangle is shown in the CFP-YFP FRET channel. FRET efficiency between RAGE-YFP and Δ DAD-DIAPH1-CFP was $10 \pm 3\%$, whereas acceptor photobleaching typically results in over a 90% decrease in fluorescence.

Table S1. Related to Figure 4 and 5. AIRs and unambiguous distance constraints used in the docking experiments.

Interaction Surfaces	Docked Domains	Active and passive AIRs		Unambiguous distance constraints
		Active AIRs	Passive AIRs	
	Chemical shift perturbations			Chemical Cross-linking
Between V and C1 domains	V domain	K110, R114, R116	auto	K107-K123 11.4Å
	C1 domain	E125, D128, S131, E132	auto	
Between C1 and C2 domains	C1 domain	L164, V165, E168, K169	auto	K62-K123 11.4Å
	C2 domain	Q268, T304, H305, S306, S307	auto	K110-C234 11.4-32.5Å P323-P323 50Å*
Between V domain and Ca ²⁺ -S100B	V domain	K43, K44, A101, M102, N103, R104, N105, G106, K107	auto	K110-K48 11.4Å
	Ca ²⁺ -S100B	E43, L44, E45, E49, A78, T81, A83, H85, E86, F87, F88, E89, H90	auto	

* This constraint is based on the observation of FRET between RAGE-CFP and RAGE-YFP expressed in HEK293 (Xie, J., *et al.* (2008) Structural basis for pattern recognition by the receptor for advanced glycation end products (RAGE). *J. Biol.Chem.* **283**: 27255-27269).

Table S2. Related to Figure 4 and 5. Statistics of the docked complexes.

Parameter	sRAGE dimer ^a	Ca²⁺-S100B-sRAGE ^b
No. of clusters	1	4
Best cluster ^c	1	3
No. of structures	200	196
iRMSD ^d	2.7	6.2
lRMSD ^e	6.6	17.2
fnat ^f	0.56	0.25
HADDOCK score	-87.6 +/- 1.5	-132.8 +/- 2.6

^a: sRAGE homo-dimer structure.

^b: S100B dimer binding to sRAGE .

^c: The cluster with the lowest average HADDOCK score. The number refers to the rank in cluster size.

^d: Interface RMSD, iRMSD, (within 10 Å of the interface) calculated from the backbone atoms of all residues involved in intermolecular contact.

^e: Ligand RMSD, lRMSD, calculated from the backbone atoms of all molecules after fitting to the backbone atoms of the first molecule.

^f: The fraction of native contacts is calculated by counting all residue contacts between each interacting protein in the reference structure and comparing how many are used in the average structure calculation for each cluster.